MOLECULAR DYNAMICS SIMULATION OF THE EFFECT OF PARTICLE HARDNESS ON TRIBOLOGICAL PROPERTIES OF NANOFLUIDS

by

CANG XU

A dissertation submitted in partial fulfillment of the
requirements for the degree of

DOCTOR OF PHILOSOPHY IN MECHANICAL ENGINEERING

2022

Oakland University
Rochester, Michigan

Dissertation Advisory Committee:

Gary C Barber, Ph.D., Chair
James David Schall, Ph.D., Co-Chair
Ankun Yang, Ph.D
Hongwei Qu, Ph.D
Peng Zhao, Ph.D

To my mother, father, sisters and friends

ACKNOWLEDGMENTS

First and foremost, I gratefully appreciate the help of my Ph.D advisor Dr. Gary Barber for his guidance in the past years during my PhD project. Besides my advisor, I would like to appreciate my co-advisor Dr. James David Schall for his contributions of time, ideas, and support on my research. Also, I would like to give my sincere thanks to my committee members for their important advices for my PhD research.

Special thanks should go to my husband, Peng Zhang, who accompanied and helped me to move forward when I met discourages since I started writing this dissertation.

Last but not the least, I would like to express my deepest gratitude to my parents, Guanglan Hua and Dezheng Xu. Without their encouragement I cannot finish my Ph.D. They are my first teacher and will support me all my life.

Cang Xu

ABSTRACT

MOLECULAR DYNAMICS SIMULATION OF THE EFFECT OF PARTICLE HARDNESS ON TRIBOLOGICAL PROPERTIES OF NANOFLUIDS

by

Cang Xu

Adviser: Gary Barber, Ph.D.

The determination of physical properties of nanofluids is mature, but the knowledge of tribological properties of nanofluids is limited. In this paper, the effects of surface roughness, fluid thickness, nanoparticle hardness, and number of nanoparticles on friction are explored systematical using a 2D Lennard-Jones molecular dynamics model. LJ parameters were chosen such that the ratio of stiffness of the nanoparticles to the opposing surfaces was approximately equal to ratio of stiffness of either aluminum oxide or zinc oxide to steel. A total of two hundred and twenty configurations were investigated. The results show that the benefits or drawbacks of nanofluid lubricants are sensitive to the friction regime (boundary, mixed, or hydrodynamic). When nanoparticles are present in lubricant-starved boundary conditions (fluid thickness less than the surface roughness amplitude), nanoparticles offer support that keeps the opposing surfaces separated. This separation results in reduced contact between the opposing surfaces and provides surface smoothing, which in turn lowers friction relative to the base fluid. At intermediate levels of fluid thickness where the fluid thickness and roughness are

approximately equal, the presence of nanoparticles has a detrimental effect on friction. Nanoparticles jam and lock surfaces together and increase friction relative to the base fluid. As fluid thickness increases, the friction of the nanofluid generally remains higher than the base fluid likely due to the increased viscosity of fluid due to the presence of the nanoparticles. This work suggests nanofluids may offer limited benefits under specific lubrication conditions, but are detrimental under most conditions.

TABLE OF CONTENTS

TABLE OF CONTENTS—Continued

TABLE OF CONTENTS—Continued

LIST OF TABLES

LIST OF FIGURES

LIST OF FIGURES-Continued

LIST OF FIGURES-Continued

LIST OF ABBREVIATIONS

CuO	Copper Oxide
ZnO	Zinc Oxide
Al_2O_3	Aluminum Oxide
ZrO_2	Zirconium Oxide
SiO_2	Silicon Dioxide
MEMS	Micro-Electro-Mechanical Systems
COF	Coefficient of friction

CHAPTER ONE

INTRODUCTION

Since first introduced in 1995 by Choi [1], nanofluids have captured the interest of researchers from engineering science, biological science and pharmacology. A nanofluid is a fluid produced by adding nanometer sized particles in base fluid. Nanofluids can be used in a large varieties of industry areas, from energy production to transportation and in electronics systems such as MEMS, microprocessors and in the field of biotechnology. In addition to enhancing thermal conductivity, heat flux and heat capacity, nanofluids could help in improving tribological properties by reducing friction and wear [2-10].

It is well known that friction and wear are particularly high in boundary and mixed lubrication compared with hydrodynamic lubrication. To date, despite many experimental studies have been carried out to investigate the tribological properties of lubricants with variety types of nanoparticles, it is still impossible to know the correlation between nanoparticle concentration, size, composition, morphology and nano-lubricant properties. The primary aim of this research is to explore the lubrication mechanism.

The objective of this research is to investigate the effects of the ratio of nanoparticle hardness to surface hardness on the tribological properties by molecular dynamics (MD) simulation method. We want to see whether particles roll, embed or smear to provide load bearing films or polish the surfaces. Research will be carried out to determine if particles and surfaces with similar hardness (hard-hard or soft-soft) the particle is more likely to roll, soft particles on hard surfaces are more likely to smear,

hard particles on soft surfaces more likely to embed or polish.

Following this, chapter two consists of a literature review of the thermal and tribological studies of nanofluids. Chapter three provides the details of the simulation method. Chapter four will be the results and chapter five contain the conclusions and future work.

CHAPTER TWO

LITERATURE SURVEY

In this section, some basic information about nanofluids and nanoparticles is introduced first. Then a review of published papers as to the tribological properties of nanofluids is given. Third, the application of molecular dynamic simulation methods is discussed.

2.1 Nanofluids characteristics

In recent decades, many nanofluids experimental studies have been done to determine the tribological properties of nanofluids made by dispersing different kinds of nanoparticles in different base fluids. Nanofluids have been widely used as heat transfer nanofluids, process nanofluids, surfactant nanofluids, chemical nanofluids, environmental nanofluids, medical nanofluids and tribological nanofluids. Researchers believed that nanofluids performed well in tribological properties when compared with traditional lubricants [11].

2.1.1 Nanoparticles types

Studies have shown that a variety of factors such as the size, concentration and morphology of nanoparticles have great impact on the tribological properties of nanofluids.

A variety of metallic nanoparticles including Cu, Ni, Al Pb and metal oxides like Co_3O_4, CuO, Fe_3O_4, ZnO, TiO_2 and Al_2O_3 are used as lubricant additives due to their special chemical and physical properties. The metal nanoparticles have some lubrication mechanisms like the formation of tribo-film or adsorption film, the rolling effect, and the

sintering or repair effect. Copper nanoparticles with small particle size, desired ductility and low melting point are widely used as anti-wear (AW) and friction modifiers (FM) compared to other products [4].

Peng et al. prepared liquid paraffin with SiO_2 nanoparticles of mean diameters 58, 140, 215, 281, 362, 420 and 684 nm respectively and studied the tribological properties using a ball on ring test. It was found that the SiO_2 nanoparticles with small size as an additive in liquid paraffin display the best load carrying capacity, friction reduction and anti-wear properties when compared with other base paraffin or base liquid mixed with large SiO_2 nanoparticles. It was found that a thin tribo-film was formed by nanoparticles deposited on the rubbing surfaces during the test [5].

Kato conducted a pin on disc wear test employing Fe_2O_3 particles with four different mean diameter sizes: 0.03, 0.3, 0.5 and 1.0 μm. Similar to that observed in a test where no particles were applied, no severe running in to mild wear transition occurred and a wear curve was produced in a test using Fe_2O_3 particles of 1.0 μm. On the other hand, the sliding distance of the severe to mild wear transition was reduced when fine particles with diameters of 0.5 and less were supplied [9].

Kato et al. studied the influences of type and size of supplied particles on the formation of tribo-films and the transition to mild wear. It was clearly observed that severe to mild wear transitions after sliding for a certain distance when Bi_2O_3 (particle diameter: 51 nm), CuO (48 nm), Fe_2O_3 (30 nm) or SnO_2 (21 nm) particles were introduced onto the surfaces. However, the addition of Mn_2O_3, TiO_2, ZnO, Al_2O_3 and SiO_2 nanoparticles has no effect for the wear reduction, which means that the wear transition behavior depends on the type of supplied oxide. The mild wear is due to

formation of the wear-protective tribofilm on the rubbing surfaces, especially for Bi_2O_3, resulting in a very small total wear volume after a relative short sliding distance [17].

Hu et al. performed molecular dynamics simulations to study the friction of the nanofluids in shear flow field. With a given volume concentration of nanoparticles, the transition pressure and load-carrying capacity increase with the decrease of the radius of the nanoparticles, due to the stronger nanoparticles' micro-motions and volume effects. After the phase transition, the shear stresses decrease with the decrease of the size of the nanoparticles [33].

2.1.2 Nanofluids dispersion stability

Robert Brown and Albert Einstein first observed the random Brownian motion of particles when they are added to a liquid medium in 1905. The nanoparticles in suspension probably accumulate and form larger conglomerates, resulting in sedimentation and in the loss of friction reduction and anti-wear efficiency. In order to obtain a reliable lubrication effect, dispersion stability is greatly required. For the stable dispersion stability of nanofluids, a variety of dispersion methods could be used such as agitation using ultrasonic shaker, magnetic stirring, chemical agitation, agitation using mechanical ball milling agitation and stirring using ultrasonic probe [10].

Stability means that the particles do not gather together at a significant rate. A stable suspension is considered as a prerequisite for an effective nanolubricant formulation. In a reciprocating test, Rabaso et al. studied two cases of ‘‘not stirred’’ and ‘‘stirred’’ inorganic Fullerene-like nanoparticles added in lubricants both exhibiting lower friction coefficients, due to the homogeneous tribo-film created on the contact surfaces with a continuous nanoparticle contact [6].

2.2 Tribological effect of nanofluids

The characteristics of nanoparticles such as size, shape, and concentrations can significantly influence the tribological properties of nanofluids.

2.2.1 Friction and wear reduction

Gara and Zou showed that friction reduction was observed by adding nanoparticles to water or oil on water-based and oil-based nanofluids. It was observed that the friction reduced obviously for smooth surfaces but reduced only slightly for rough surfaces when ZnO and Al_2O_3 nanoparticles were added into the water based nanofluids. As to oil-based nanofluids with ZnO nanoparticles, the friction and wear for smooth surfaces were reduced. For lower the velocity and load, the friction reduction was enhanced [12,13].

Ma et al. investigated the effect of ZrO_2 nanoparticles on the friction and wear behavior of MACs base oil. ZrO_2 nanoparticles as additives to MACs base oil have a slight effect on its friction, but significantly improve its wear performance and load carrying capacity. In the friction process, inorganic ZrO_2 nanocores were deposited on the rubbing surfaces to form a ceramic-like boundary film, while active element P in TOPO had tribo-chemical reaction with the rubbing surfaces, forming an easily sheared protective film of $FePO_4$. The synergistic action of both ceramic-like ZrO_2 boundary film and $FePO_4$ protective film prevented severe wear and seizure and damped the tribological impact [15].

Battez et al. studied the anti-wear behaviour of CuO, ZnO and ZrO_2 nanoparticles suspensions in a polyalphaolefin (PAO 6). All nanoparticle suspensions exhibited friction and wear reduction compared to the base oil. ZrO2 and ZnO suspensions exhibited

similar friction and wear behavior as a function of nanoparticle content, which contrasts with CuO. The suspensions with 0.5% of ZnO and ZrO_2 had the best general tribological behaviour, exhibiting high friction and wear reduction values. However, CuO suspensions had the highest friction coefficient and lowest wear for the same nanoparticle content (2%). Friction and wear behavior should both be considered when designing lubricants because both parameters can exhibit different tendencies depending on additive content. The size and hardness of the nanoparticles should be taken into account when the additives are solids. In the experiment, CuO, ZrO_2 and ZnO nanoparticles have been applied to exhibit reduction in friction and wear at all low concentrations compared to the base oil, showing that the optimal concentration for ZnO and ZrO_2 nanofluids were 0.5%, and the suspension with 2% CuO exhibited the best anti-wear performance and the lowest anti-friction effect [16].

Guo et al. focused on the use of ionic liquid as a nanofluid surfactant by investigating oil based ZnO and WS_2 nanofluid tribological properties using two different surfactants: oleic acid (OA) and ionic liquid (IL). ZnO/IL nanofluids generally reduced wear and had better wear performance than WS2/IL. Nanofluids with oleic acid as surfactant will generally reduce COF. The maximum COF reduction of ZnO/OA nanofluids and WS_2/OA nanofluids are almost the same, which is approximately 8.7%; however, the coefficient of friction reduction is not significant with addition of nano particles. The addition of OA mainly reduced the friction. It was found that using phosphinate ionic liquid alone as an oil additive did not improve nanofluid tribological performance. Meanwhile, oleic acid when used as a surfactant had lower friction and reduced wear for both ZnO nanofluids and WS_2 nanofluids [18].

Ma et al. studied the anti-wear and friction performance of ZrO_2 nanoparticles as a lubricant additive. The results showed that the friction coefficient and wear volume were reduced to some extent. It showed that the average friction coefficient decreased by 27.34%, and that the weight loss of the thrust-ring indicated no wear or negative wear, the wear loss after six loads tests being −0.0163 g. The anti-wear (AW) and reducing friction (RF) abilities of the oil with ZrO_2 nanoparticles addition were considerably improved, maximizing at an additive concentration of 0.5 wt% [19].

Zulhanafi et al. conducted a test using a nanolubricant mixed by palm kernel oil (PKO) with copper oxide nanoparticles revealed 8.73% and 20.12% lower COF than palm kernel oil and mineral based engine oil (SAE 40) respectively. Meanwhile, PKO+CuO exhibited 1.74% and 10.13% larger wear scar diameter when compared to palm kernel oil and mineral based engine oil (SAE 40) separately. However, even with higher wear scar diameter, the palm kernel oil with copper oxide nanoparticles have smoother surface roughness compared to PKO and SAE 40 [21].

2.2.2 Tribological mechanism

Stott and coworkers have studied the role of tribo-particulates in dry sliding process, a large of amount of heat is released with heavily deformed wear debris, thus enhancing the oxidation of the fine wear debris particles. It is shown that the wear-protective compact particle layers are produced on the rubbing surfaces by strong adhesion produced between the contacting metals and is beneficial to the decrease in friction and wear [7-8].

Wu et al. reported that nanoparticles including Nano-diamond, CuO and TiO_2 used as additives in lubricating oils exhibit good friction reduction and anti-wear

behavior, especially for CuO. In the friction-reduction test, compared with the oils without nanoparticles, the friction coefficients were decreased by 18.4 and 5.8% when CuO was added to the SF oil and the base oil. As to the anti-wear test, compared to the oils without nanoparticles, when CuO was added to the SF oil and the Base oil, the worn scar depths were reduced by 16.7 and 78.8%. The author believed that the anti-wear effect is attributed to the tribo-film created by the deposition of CuO nanoparticles on the worn friction surface [14].

Kato et al. carried out the wear tests at room temperature and observed tribo-sintering of the supplied Fe_2O_3 particles, which produced "tribofilms" to prevent direct metal contact and to work as load bearing areas. The formation of wear-protective tribofilms produced by tribosintering of the supplied oxide particles on the rubbing surfaces caused the transition from severe to mild wear. Sintering is a process whereby particles bond together at temperatures typically below the melting point, by atomic transport events [17].

Chen et al. investigated the tribology properties of ZnO/Al_2O_3 composite nanoparticles as additives in liquid lubricants by the thrust-ring and the fourball test. Owing to the combined effect between ZnO and Al_2O_3 nanoparticles, the ZnO/Al_2O_3 composite nanoparticles as lubricant additives exhibit 26.2 and 37.5% reduction in wear scar diameter and COF when compared with the pure ZnO and Al_2O_3 lubricating oil. By turning the sliding friction into rolling friction and forming a hard Al_2O_3 protective film after transferring to the friction surface, the ZnO/Al_2O_3 nanoparticles composite improved the tribology properties [20].

2.3 Molecular dynamic simulation method

For more than two decades, nanofluid experimental studies related to metal, metal oxides, ceramic and polymeric nanoparticles dispersion in different base fluids have been done to undermine different properties of base fluids modified with nanoparticles. There are many variable parameters and different nanoparticles being used. Extensive material usage, high technical expertise and extensive time are required for performing each experiment. Most of the published research on friction and wear reduction was conducted by experiment methods. Due to the expensive and time-consuming drawbacks, molecular dynamic (MD) simulation method has become an effective approach for nanofluid simulation over the last decades.

2.3.1 Molecular dynamic simulation on the rheological property

Molecular dynamic simulation method has been applied in a variety of areas, such as the mechanism of nanoparticle in improving load carrying capacity of lubricant film and the study of mechanical effects of lubrication on a nanoscale contact process.

Loya et al. employed a largescale molecular thermal dynamic program (i.e. LAMMPS) to simulate the movement of nanoparticles in the fluid with the COMPASS force field with smoothed particle hydrodynamic potential (SPH) and discrete particle dynamics potential (DPD) to investigate rheological properties of CeO2-water nanofluid. The simulation values with a series of iteration agreed within 5% of the experimental results, showing that 10 % CeO2 nanoparticles dispersion in water has a viscosity of 2.0–3.3 mPas [28].

Hu et al. studied the properties of base oil and nano-lubricant film confined between two approaching walls under boundary lubrication using molecular dynamics

simulation. The nano-lubricant was composed of one Cu nanoparticle and n-octane as base fluid. It was found that the load-carrying capacity of nano-lubricant was much higher than that of the base oil. The effect of nanoparticles on lubricant film structures was analyzed to determine mechanisms responsible for these results. The results showed that the nano-lubricant molecules become more organized and compact compared with base oil because of an adsorption layer around the nanoparticle. What's more, the soft Cu nanoparticle was deformed by the structural characteristics of the nano-lubricant film, which provided good support for the lubricant film. The results indicated that the nanoparticle improved the load-carrying capacity before rupture of the lubricant film [30].

Stephan et al. investigated the effect of a lubricant on nano-indentation and -scratching of a Fe (100) surface of a dry and lubricated contact process by molecular dynamics simulation. The lubricant was modeled as a Lennard-Jones fluid. By comparing a dry reference case with two lubricated contacts-differing in the adsorption strength of the lubricant-the effects of the lubricant can be identified. Two lubricated scenarios, differing in the solid–fluid interaction energy, are compared with a dry one. It was found that the fluctuations in the time evolution of the friction forces, the total dislocation length and the chip formation were reduced by the lubricant. The reduction increases significantly with the adsorption energy due to a mechanical coupling between the indenter and the substrate atoms via the lubricant which balance force peaks [31].

Rajabpour et al. employed molecular dynamics simulation method to construct the modeling for calculating the specific heat of water-Cu nanofluids compared with the mentioned theoretical models. The nanofluids with five different nanoparticles volume

concentrations 2%, 4%, 6%, 8%, and 10% were considered in the simulation, with the diameter of copper nanoparticles setting to 2 nm. The obtained results show that with the increasing nanoparticles volume fraction the specific heat capacity of Cu-water nanofluids gradually decreases. The obtained MD simulation results and the calculated specific heat thermal equilibrium model prediction exhibit good agreement when compared with two existing applied models [34].

2.3.2 Molecular dynamic simulation on the tribological property

In contrast with the experiment method, the simulation method was seldom used in the tribology process. The former MD simulations were mostly related to self-diffusion of fluids, mixing of oil with water to create emulsions, protein bi-layer and polymeric diffusions. In this research, MD simulations will be used to study and examine the tribological mechanism of nanofluids in more detail.

Hu et al. investigated the frictional properties of two hard nanoparticles (diamond and silicon dioxide) confined by two iron blocks and revealed the underlying mechanisms using molecular dynamics simulation. Under a low load (500 MPa) and a low sliding velocity (10 m/s), the two iron blocks were separated by the diamond and SiO_2 nanoparticles and the nanoparticles worked as ball-bearings and converted the sliding friction into mixed friction consisting of both sliding and rolling， resulting in improved deformation, temperature distribution and friction force. When the load was increased to 1000 MPa, the deformation of the SiO_2 nanoparticle induced the loss of the rolling effect, but the tribology properties of diamond changed slightly. Under a low load (500 MPa) and a high velocity (500 m/s), a transfer layer was formed without nanoparticles. However, the SiO_2 nanoparticle only supported the surfaces for a certain time and the

diamond nanoparticle prevented direct contact during the entire simulation [32].

In this research conducted by Hu and his coworkers, the interactions between nanoparticles and the base fluid were investigated by MD simulations. Their results revealed the effects of nanoparticles on the frictional behaviors of lubricant films. At low loads, compared to the base fluid, the shear stress of the nanofluids is larger due to the higher viscosity. While at high loads, for both the base fluid and the nanofluids films phase transition occur in the lubricant film. What's more, the shear stress of the nanofluids is lower than that of the base fluid when the load is higher exceeding the base fluid transition pressure. In the process of flowing, the interactions between nanoparticles due to the collision or agglomeration of nanoparticles contribute to shear stress. For now, the impact that such collisions have on the friction properties of nanofluids are unable to be quantified, and we are unclear about the collision probability between nanoparticles [33].

Hu et al. used the molecular dynamics approach to study the effects of nanoparticles on tribological properties at various temperatures in two cases, one with and the other without Cu (copper) nanoparticles. The results revealed that surface abrasion and temperature distribution were significantly improved in the case with Cu nanoparticles, resulting in the improvements in tribological properties achieved by the presence of nanoparticles. The improvement in anti-wear properties for cases with Cu nanoparticles becomes more significant with an increase in the temperature of the friction pair [35].

Chandross et al. [36] studied the structural and dynamical properties of water confined between methyl-terminated and carboxyl-terminated self-assembled monolayers

(SAM) on silica substrates using MD simulation. They found that as the film thicknesses of water decreases the diffusion coefficient of water molecules decreases. What's more, within the studied range of loads, no water molecules penetrate the SAM's carboxyl-terminated hydrophobic region. The classical molecular dynamics simulation method was used to investigate the interaction of water with SAMs on amorphous silica by Chandross et al. [37]. The results indicated that a threshold radius value exist. Below the critical radius, the presence of water tends to heal damage. However, damage was magnified by the water when above the critical radius.

Lv et al. [38] used the molecular dynamic simulation method to study the impact and friction characters of nanofluids with many nanoparticles. The results showed that in the friction process, nanoparticles rotated and translated, but were also affected by the interactions of nanoparticles. During the compression process, nanoparticles tended to agglomerate, and with increased pressure, the phenomenon became more apparent. The united nanoparticles would provide supporting effects and resulted in reduced contact between two solid surfaces, which improved lubrication and decreased friction. Izadkhah et al. investigated the influence of Al_2O_3 nanoparticles on the stability and viscosity of water/EG nanofluids by the molecular dynamic simulation method. The results confirmed the complete stability of the Al_2O_3 nanoparticles in pure water. The molecular dynamics simulation results showed that the decrease in Al_2O_3 nanoparticles concentration and increase in temperature in the all studied base fluids decreased the base fluid and nanofluid viscosity, and the predicted values were in good agreement with experimental data [39].

Previous MD simulation studies related to tribological properties mostly

investigated third body nanoparticles confined between two solid walls or nanofluids consisting of nanoparticles usually having the same material with the solid walls in the unit simulation system and consequently the influences of nanoparticles' type, interactions between different materials are ignored [32, 33, 35, 38]. To-date the impact that such collisions have on the friction properties of nanofluids are unable to be quantified, and the collision probability between nanoparticles is unclear. Simulations by Aminfar et al [40] suggest that the interaction strength between nanoparticles and fluids will influence agglomeration with an increase in interaction strength leading to lower probability of agglomeration. Temperature and corresponding increase in Brownian motion may also increase the probability nanoparticle collision and hence agglomeration [41].

In this research, further studies are carried out to add to the understanding of the effects of surface roughness fluid thickness with single and multiple nanoparticles on friction properties of nanofluids. In addition, the effect of nanoparticle hardness is investigated. In what follows, first a description of a MD method and setup used in this work will be given. Then to establish a reference, a series of base fluid-only simulations that vary both surface roughness and fluid thickness will be presented. Next, these results are compared to simulations of fluids containing either a single hard or soft nanoparticle. Last simulations of fluids containing either five hard or five soft nanoparticles will be presented.

CHAPTER THREE

MOLECULAR DYNAMIC SIMULATION DETAILS

Based on the previous literature review and the experiment tests conducted by Zhou et. [42], a series of molecular dynamic simulations were setup. In order to investigate the effect of particle hardness on the tribological properties of nanofluids, four kinds of nanoparticles with different hardness values, Al_2O_3, ZrO_2, ZnO and CuO were built in this simulation.

3.1 Simulation model

Molecular dynamics simulation method was used to simulate the tribology process in order to analyze the tribological properties of nanofluids. In the simulation, the simulation model was set up according to the experimental ball-on-disk rotational test performed on the UMT-3 tribometer. The model consisted of three kinds of materials according to the tribology model: solid walls, fluid and nanoparticles. The solid walls work as a friction pair representing the ball and disc separately in the experiment. The thin lubricant films consisting of liquid lubricants and nanoparticles were confined by the solid walls.

3.1.1 Model setup

In MD computer simulations, a set of initial conditions (relative positions and random velocities of particles from Boltzmann distribution) are described and the interatomic forces are calculated using classical potential energy. The motion of atoms and molecules in a phase space of systems consisting of thousands of atoms is simulated by the numerical solution of a set of coupled differential equations based on the particles'

classical equations of motion, Newton's equation of motion:

$$F = m\frac{dv}{dt} \qquad \text{(Eq.1)}$$

where F is the force on a particle, m is its mass, v is the particle velocity, and t is the time.

Interatomic forces (F) are calculated from the spatial derivatives of the classical potential energy functions based on quantum-mechanical processes. In our simulations, the interactions are set up to mimic planar Couette flow with a fluid contained between two solid walls. The basic set-up configuration for the simulations is showed in Figure 1. The system is two-dimensional with a periodic boundary condition applied in the x-direction. The atoms within the two solid surfaces, fluid, and nanoparticles all interact through the Lennard-Jones (LJ) potential energy function.

$$v_{LJ}(r) = 4\varepsilon\left[\left(\frac{\sigma}{r}\right)^{12} - \left(\frac{\sigma}{r}\right)^{6}\right] = \varepsilon\left[\left(\frac{r_m}{r}\right)^{12} - 2\left(\frac{r_m}{r}\right)^{6}\right] \qquad \text{(Eq.2)}$$

where ε and σ are the characteristic energy and length scales, respectively and r is the interatomic distance for any given pair of atoms. In the right hand side of Equation 2, r_m is the distance at which the potential reaches its minimum. At r_m the potential function has the value –ε. Even though more accurate potentials exist, the Lennard-Jones potential has been used extensively in computer simulations due to its computational simplicity. The relative material properties for the solid, fluid, and nanoparticles and the interactions between each can be approximated by careful selection of the two free parameters ε and σ. Similar simulation methods to those described here have been

applied in the past to model fundamental friction behavior such as the origins of molecular friction, the origins of stick-slip behavior in boundary lubrication, and phase transformation and dynamics of confined fluid films [43-45]. Belita et al. [46] studied the effect of lattice type and disorder on domain wall motion in two dimensions. Nolle et al. [47, 48] studied the morphology, dynamics of interfaces and the effect of quenched disorder on moving interfaces in two dimensions in random two dimensional media. Luan et al. [49] used a hybrid simulation method to study non-adhesive contact between two dimensional self-affine rough surfaces. The current model builds on these foundational works and established methods by adding particles to the interface.

Initially, the model measures 226 by 240 in relative distance units of σ in the x- and y- directions respectively. The lubricant film thickness D was set to 0, 2, 4, 6, 8, 10, 12, 14, 16, 20, 25 σ. The diameter of nanoparticles placed in the base fluid is 20 σ.

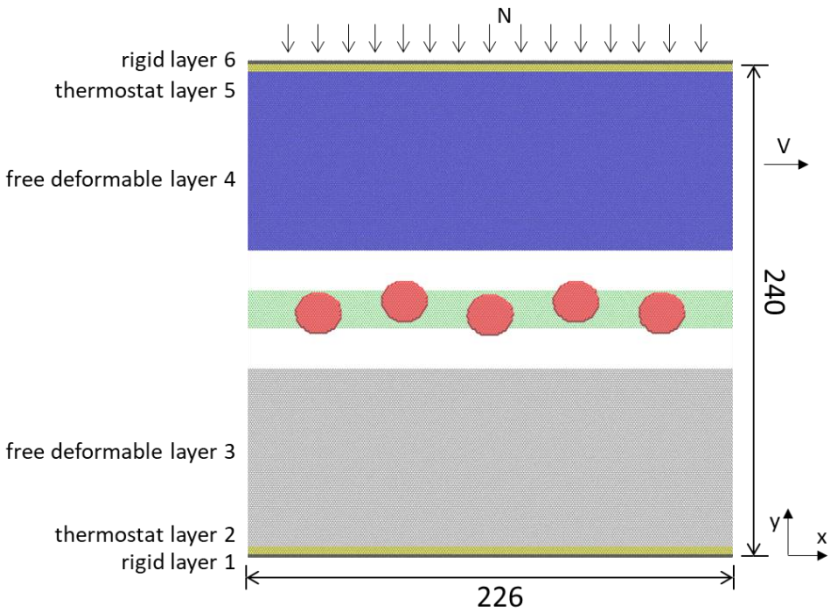

Figure 1 Model with smooth surfaces and fluid containing five particles

3.1.2 Periodic condition in MD simulation

An infinite lattice constructed to replicate the cubic simulation box throughout the domain refers to periodic boundary condition. Atom settings in a center box replicates and is a mirror image for the settings in other boxes as shown in Figure 2. A disturbance in one box matches in the other box. An atom leaving from one box enters the other neighboring box from the opposite position. Subsequently, the central box is free of any boundaries. This is particularly useful in tribology simulations. As atoms in the upper surface (see Figure 1) slide they leave the right side of the simulation box and wrap back around to the left creating what is essentially an infinite surface. This is similar to an experimental pin on disk test where the pin makes multiple passes over the disk.

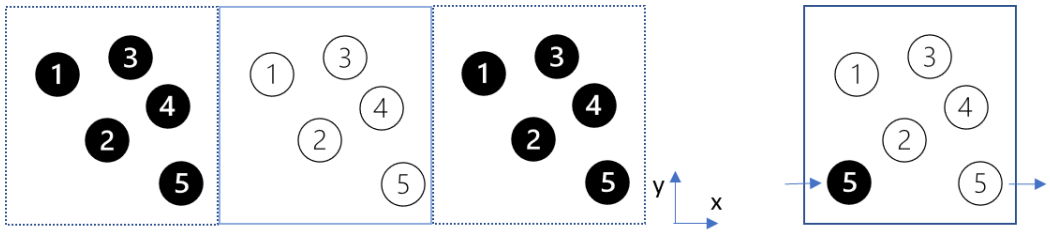

Figure 2 Periodic boundary condition of MD simulation

3.2 Generating roughened surfaces

Figure 1 shows the dimensions of simple set model consisted of two smooth solid surfaces. As suggested by Gara and Zou [12], the size of the particle relative to the surface roughness plays a role in the amount of friction reduction obtained in nanofluid lubricant systems. To investigate the effect of roughness we generated sets of roughened surfaces. The roughened surfaces are generated by superposition of sine functions of

randomized amplitude, as described by Eq. 3:

$$y = \sum_{n=n_{min}}^{n_{max}} \frac{A_n}{\sqrt{n}} sin\ (nx) \qquad \text{(Eq.3)}$$

In eq. 3, x and y are the coordinates corresponding to the surface profile, n is the frequency, and A_n is a randomized amplitude scaling factor assigned to each frequency n. Each A_n is selected randomly such that A_n varies between $-A_{max}$ and A_{max}. The parameter A_{max} is a parameter used to fine tune the root mean square (RMS) roughness value of the resulting surface. The maximum and minimum frequencies, n_{max} and n_{min} set upper and lower bounds for the wave functions that make up the surface. The values of n_{min} and n_{max} were set to 2 and 30 respectively. The factor $\sqrt{n}$ scales the amplitude so that higher frequencies play a decreasing role in the surface roughness. The y-coordinate for the surface is calculated for x ranging between 0 to 2π. The resulting surface profile is then scaled to x' over the simulation cell of length x_{box} (Eq. 3) such that it produces a surface that is periodic in the x-direction according to the following relation:

$$x' = \frac{x}{2\pi} x_{box} \qquad \text{(Eq.4)}$$

Four surface pairs were generated. A unique surface for each pair was generated by selecting different random number seeds for A_n. The amplitude scaling factor A_{max} was adjusted so that the pairs, while remaining individually unique, had approximately the same RMS roughness. The properties of each surface are described in Table 1. Spatial dimensions for A_{max}, RMS, and surface amplitude (maximum peak-minimum valley) are given LJ units of σ.

The amplitude scaling factors A_n were selected such that the roughness amplitude of each surface pair is less than (Small), approximately equal to (Medium), and greater

than (Large) the diameter of the nanoparticles (d=20) used in the nanofluids. Table 2 shows the approximate ratio of the surface amplitude relative to nanoparticle diameter for these four model pairs. The fourth pair is simply an atomically smooth (Smooth) surface with no roughness added. All models including smooth model and rough models are shown in Figure 3.

Table 1 Surface properties

Surface	Amax	Seed	RMS	Amplitude
Smooth	-		0[a]	-
Small (A)	2.5	1234	2	8.6
Small (B)	2.33	4321	1.9	9.9
Medium (A)	5	1234	3.9	17.2
Medium (B)	4.65	4321	3.9	19.7
Large (A)	10	1234	7.8	34.4
Large (B)	9.3	4321	7.8	39.3

[a] The smooth surface consists of an atomically smooth plane of atom with no added roughness.

Table 2 Ratio parameters

Parameters \ Surface Type	Smooth	Small	Medium	Large
Roughness Amplitude	0	10σ	20σ	35σ
Ratio Parameter	0	0.5	1	1.7

(a)Smooth surface (b) Small rough surface

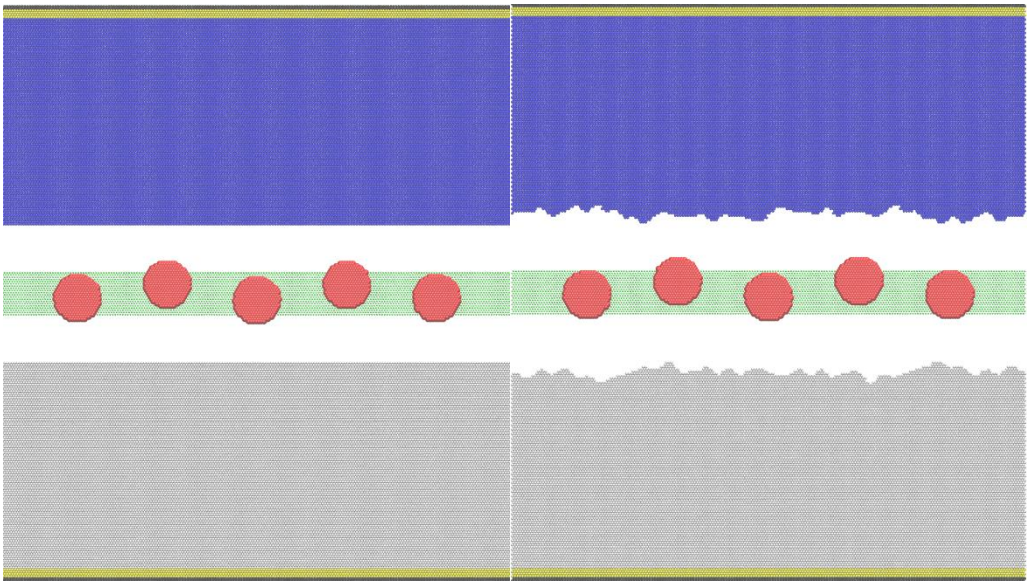

(c) Medium rough surface (d) Large rough surface

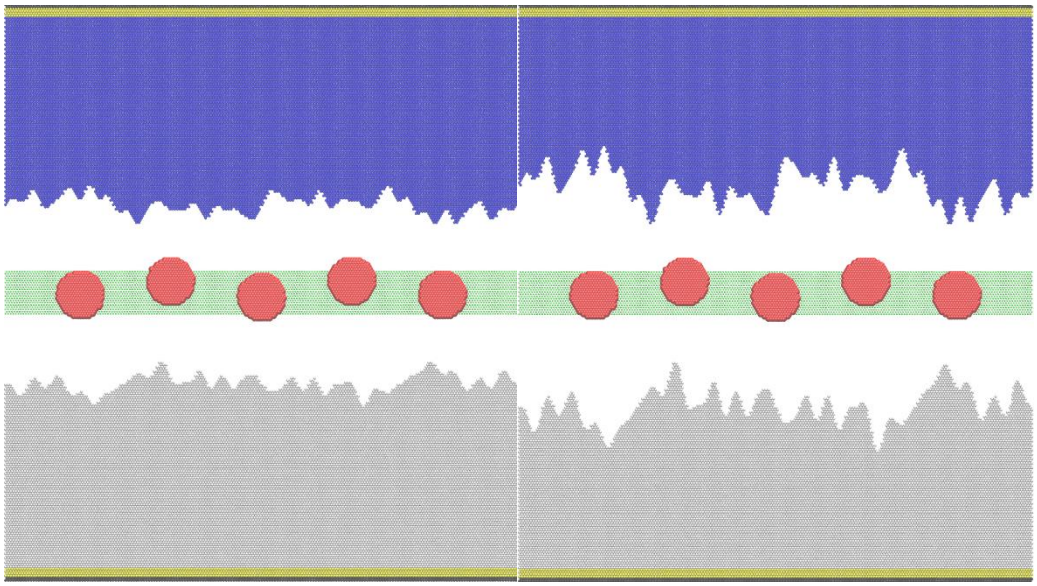

Figure 3 Starting configurations for small, medium, and large roughened A/B pairs with nanofluids. The smooth surface is shown for comparison

3.3 Selection of the interaction parameter σ and ε

In simulations utilizing LJ potentials quantities such as time, temperature, force, etc. are usually expressed in unitless quantities given in terms of multiples of the characteristic energy ε and characteristic length σ [50]. The relative material properties such as stiffness and strength can be assigned by adjusting the parameters σ and ε. In this work we set the characteristic energy ε and characteristic length σ for the two solid surfaces equal to one. The simulation temperature (T*=Tk_b/ ε) was reduced to 0.1 so that the walls remain solid. The ε values for nanoparticles and base fluid where then adjusted relative to the solid surfaces to produce a relatively hard particle and a viscous fluid, respectively. The characteristic length σ was set to 1.0 and 1.12 for the particle and base fluid, respectively. The ratio of $\varepsilon_{particle}$ / $\varepsilon_{surface}$ was set to eleven, which is approximately the same ratio as that of the hardness of an aluminum oxide nanoparticle to a steel surface [51]. The ratio of $\varepsilon_{fluid}/\varepsilon_{surface}$ was set to 0.1. At temperature of T*=0.1 and characteristic length of 1.12, an $\varepsilon_{fluid} = 0.1$ falls in the fluid region of the LJ phase diagram [52]. The next step is to determine the interaction parameters for unlike atom pairs, *i.e*. between the fluid and surfaces, fluid and nanoparticles, and nanoparticles and surfaces. Traditionally Lorentz-Berthelot rules are used to determine the interaction parameters for pairs of unlike particle types, i and j, where $\varepsilon_{ij} = \sqrt{\varepsilon_i \varepsilon_j}$ and $\sigma_{ij} = (\sigma_i + \sigma_j)/2$. Here, however, we have assumed an ε = 0.1 for all unlike particles in the simulation. This represents a weak interaction between unlike pairs which results in low adhesion between the fluid, nanoparticles, and the surface pairs. A cut-off distance of 2.5σ was assumed for all interactions. Four kinds of nanoparticles with different hardness Al_2O_3, ZrO_2, ZnO and

CuO were used as nanofluid additives in the experiment of Zhou et [40]. Table 3 shows the properties of these nanoparticles. A full listing of material parameters is given in Table 4.

Table 3 Properties of Al_2O_3, ZrO_2, ZnO and CuO nanoparticles

Nanoparticle	Mohs numbers (Mohs)	Size (nm)	Shape
Al_2O_3	9	45-50	Nearly spherical
ZrO_2	8	20-30	Spherical
ZnO	4.5	10-30	Nearly spherical
CuO	3-4	23-37	Nearly spherical

Table 4 Model interaction parameters for all materials

Interaction Type	Vickers Hardness (kg/mm^2)	Epsilon (ε)	Characteristic Length (σ)	Cut-off distance
Substrate	177	1	1	2.5σ
Nanoparticle Al_2O_3	2000	11	1	2.5σ
Nanoparticle ZrO_2	1381	8	1	2.5σ
Nanoparticle ZnO	266	1.5	1	2.5σ
Nanoparticle CuO	142	0.8	1	2.5σ
Fluid	-	0.1	1.12	2.5σ
Substrate-Particle	-	0.1	1	2.5σ
Substrate-Fluid	-	0.1	1	2.5σ
Fluid-Particle	-	0.1	1	2.5σ

3.4 Molecular dynamics simulation method

To generate Couette flow the top wall is moved in the +x-direction relative to the lower wall while a constant load is applied between the two surfaces in the y-direction. The two solid blocks were divided into six layers: rigid layers (1,6), thermostat layers (2,5), and free deformable layers (3,4). The MD simulation proceeds in three stages: thermalization, loading, and sliding while loaded. First, all atoms in the thermostated and free deformable layers are thermalized for 100,000 timesteps. An MD time step of 0.005τ where $\tau = (\varepsilon/m\sigma^2)^{1/2}$ was applied. The temperature was held constant using a Berendsen thermostat [53] at a reduced temperature T*=0.1 as described in Section 3.3 above. Second, an average downwards force of 0.05 ε/σ was applied to each atom in the top rigid layer to simulate an external normal loading condition. The bottom rigid layer is held stationary to prevent translation of the system. Thermostating was applied away from the interface on layers 2 and 5. The atoms in the free deformable layers, fluid, and nanoparticles were unconstrained and moved freely according to Newton's 2nd Law. Once equilibrium load and temperature were reached, sliding of the top solid relative to the bottom solid was initiated by applying a constant velocity of 0.1 σ/τ. The simulation was then run for $8x10^6$ time steps which is sufficient for the periodic image of the top solid to pass over the lower solid approximately eighteen times. The normal and friction forces are output every 4000 time steps during sliding. To avoid undue influence from the thermostat on the friction forces measured during sliding, thermostating was turned off in the sliding direction in accordance with Robbins and Muser [54]. All simulations were run using Sandia's Large-scale Atomic/Molecular Massively Parallel Simulator (LAMMPS) [55] and visualized using Visual Molecular Dynamics (VMD) [56].

Figure 4 is the flow chart of the procedure for the molecular dynamic simulation. After the setup of the model, the molecular dynamic simulation technique was employed to equilibrate the system from its unstable position to stable position. Implementing force field causes the movement of the atoms in the system. Later, the pair potential computes particular behavior that is required to fulfil the simulation.

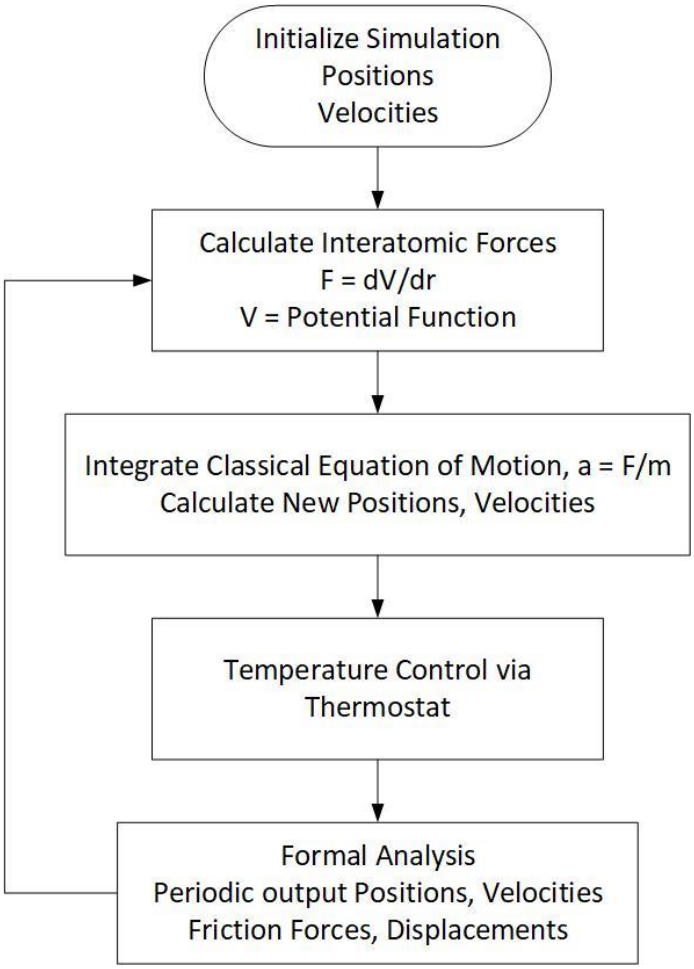

Figure 4 Flow chart of molecular dynamic simulation

CHAPTER FOUR

RESULTS AND DISCUSSION

4.1 Effect of surface roughness

There are four pairs of solid surface models with different surface roughness: smooth (Sm), small (SR), medium (MR) and large (LR) rough surfaces, in which smooth surface is simply an atomically smooth surface with no roughness added. Throughout this research, smooth surface model is used as a comparison because smooth surface usually does not exist in the laboratory experiment.

4.1.1 Models with base fluid

Models built with base fluid without any particles confined between smooth (Sm), small (SR), medium (MR) and large (LR) roughness surfaces were studied first. Figure 5 shows the evolution of friction force with respect to sliding time step for the base fluid for fluid thickness of zero, two, four, and six units, respectively. Friction generally starts high and evolves towards a lower steady state value as the simulation progresses. As described in the procedural section above, the average friction force is taken from the last two thirds of the sliding time. As expected under dry conditions, when no fluid is present, friction is highest. For the smooth surface with no fluid, the friction force approaches the theoretical interfacial shear strength of the base material. As illustrated in Figure 6, the average friction force drops significantly when a fluid is introduced into the interface and the role of roughness is reversed. With fluid present, smoother surfaces exhibit lower friction relative to rougher surfaces once the fluid thickness is greater than or equal to 4σ. As fluid thickness increases the friction for all levels of roughness converges towards a

single low value as the lubrication regime transitions from boundary to mixed to hydrodynamic. Visualization snapshots from the last frame of the MD trajectories for systems with fluid thickness of 0, 4, 8, and 12σ are shown in Figure 7. Generally, for all systems under study, thicknesses greater than 14σ are sufficient to enable full-fluid film lubrication and prevent any surface to surface contact at any level of roughness. For brevity the configurations with fluid thickness greater than 14σ are not shown since they do not provide much additional insight. The visualizations in Figure 7 show combinations of wear and smoothing of the asperities, fusion of the surfaces, shear, and generation of third body particles. During dry contact the materials only interact at the asperity peaks and the friction of the rougher surfaces is lower than for smooth surfaces due to the difference in true contact area. Transfer films and third body wear particles were formed in all the rough surface models during dry contact. The scatter in the average friction force for the large and medium roughness surfaces at low fluid thickness (for example the anomalously high friction for rough surfaces at fluid thickness 10σ) is attributed to the stochastic nature of bonding between the opposing surfaces. This is consistent with previous work [57]. This variability is reduced as fluid thickness is increases and hence interaction between opposing surfaces is decreased.

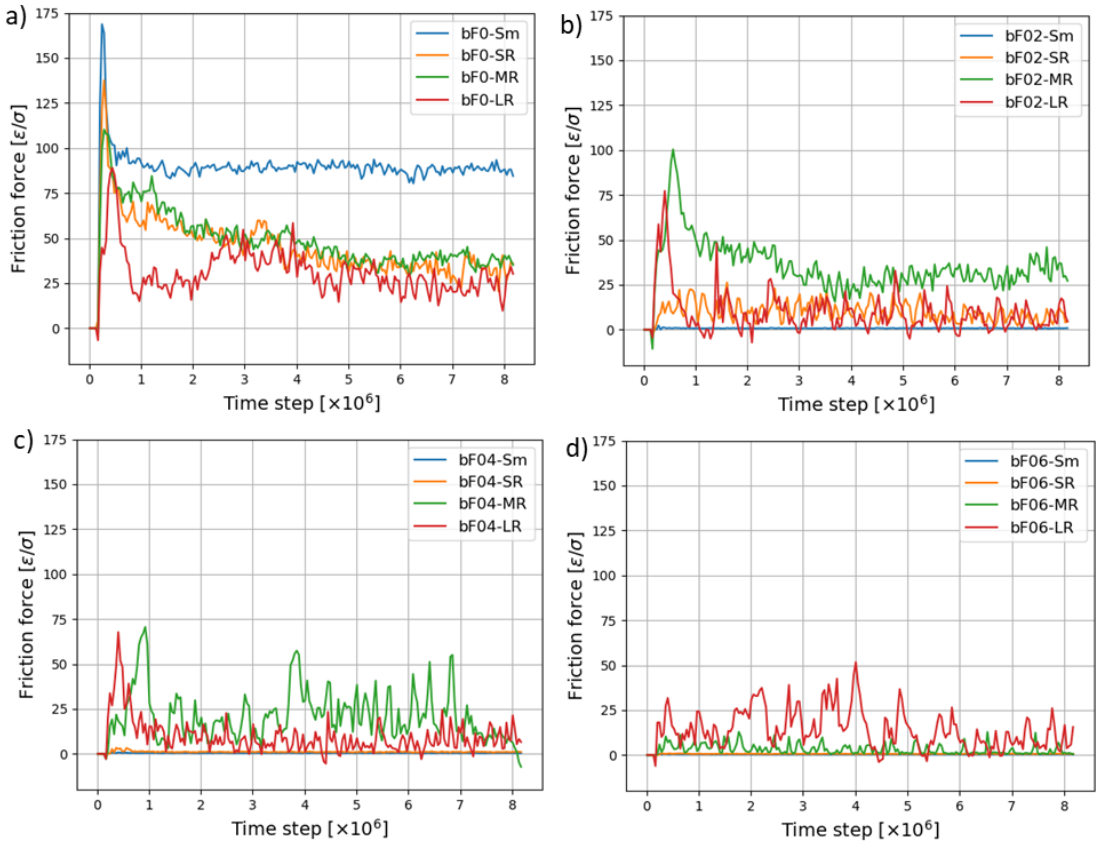

Figure 5 The friction force with respect to sliding time step for base fluid model with liquid with the thickness of (a) 0, (b) 2, (c) 4 and (d) 6 σ confined between smooth (Sm), small (SR), medium (MR) and large (LR) roughness solid surfaces

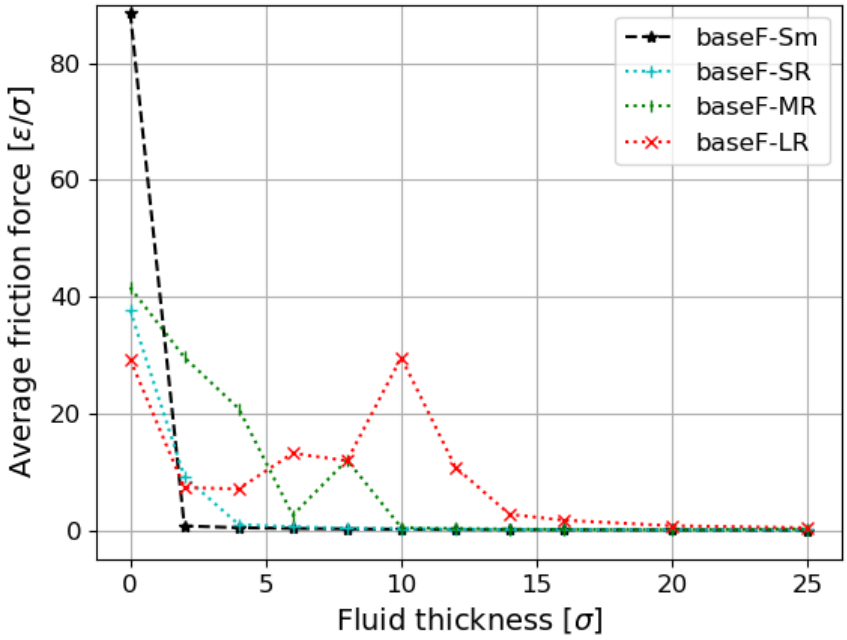

Figure 6 Friction force as a function of fluid thickness for base fluid model

Thickness / Surface	0 layers	4 layers	8 layers	12 layers
Smooth	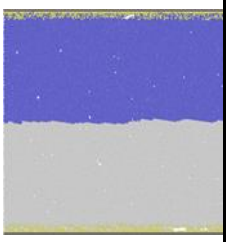	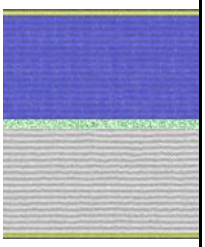	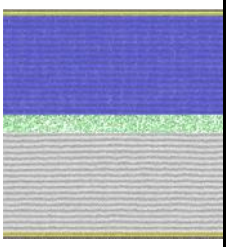	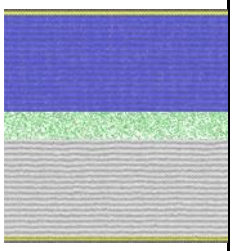
Small	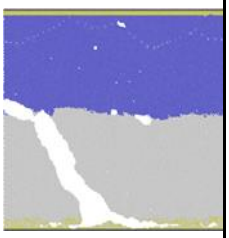	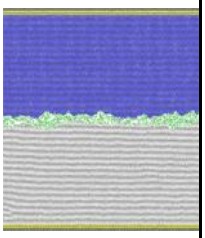	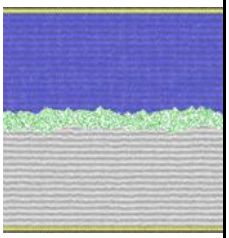	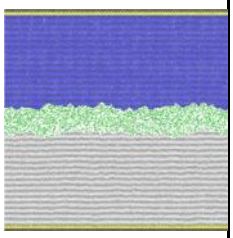
Medium	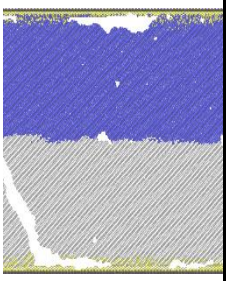	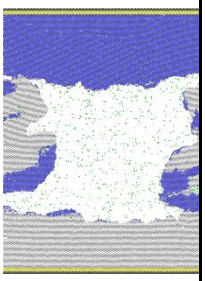	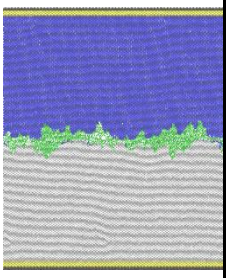	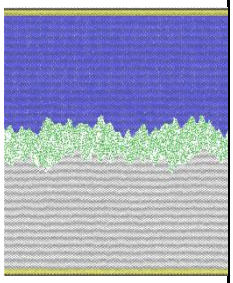
Large	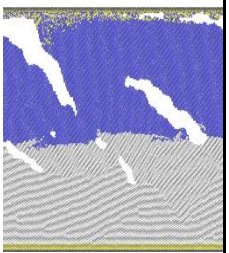	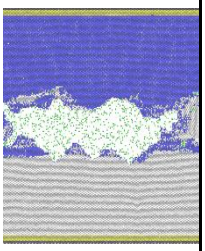	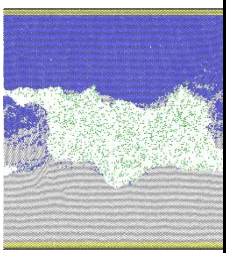	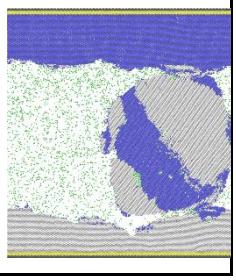

Figure 7 Final state images for base fluid model with liquid with the thickness of 0, 4, 8, 12 σ confined between smooth, small, medium, and large roughness solid surfaces

4.1.2 Models with single Al_2O_3 nanoparticle

To investigate how of the addition of a nanoparticle influences friction, models were constructed with either a single hard or soft nanoparticle. The nanofluid was confined between Sm, SR, MR and LR surfaces and the fluid thickness was varied. Figure 8 shows the evolution of friction force with respect to sliding time step for the one Al_2O_3 particle nanofluid for fluid thickness of zero, two, four, and six units, respectively. Except for no fluid models, the smooth surface models with one particle nanofluid always show the lowest friction force. When the fluid thickness is equal to or greater than 4σ, the friction force reduces as the roughness decreases, which can be seen from Figure 9. Visualization of the MD trajectories shows the nanoparticle prevents contact between the top and bottom surfaces as long as some fluid is present, as displayed in Figure 10.

4.1.3 Models with multiple Al_2O_3 nanoparticles

Models built with nanofluid with multiple particles confined between smooth (Sm), small (SR), medium (MR) and large (LR) roughness surfaces were studied. Figure 11 shows the evolution of friction force with respect to sliding time step for the five particles nanofluid for fluid thickness of zero, two, four, and six units, respectively. Average friction force displayed in Figure 12 shows that the friction force of the smooth surface model is always lowest except for different rough models with no fluid. As roughness increases, friction increases. Visualization of the MD

trajectories in Figure 13 shows that the particle separates the top and bottom surfaces

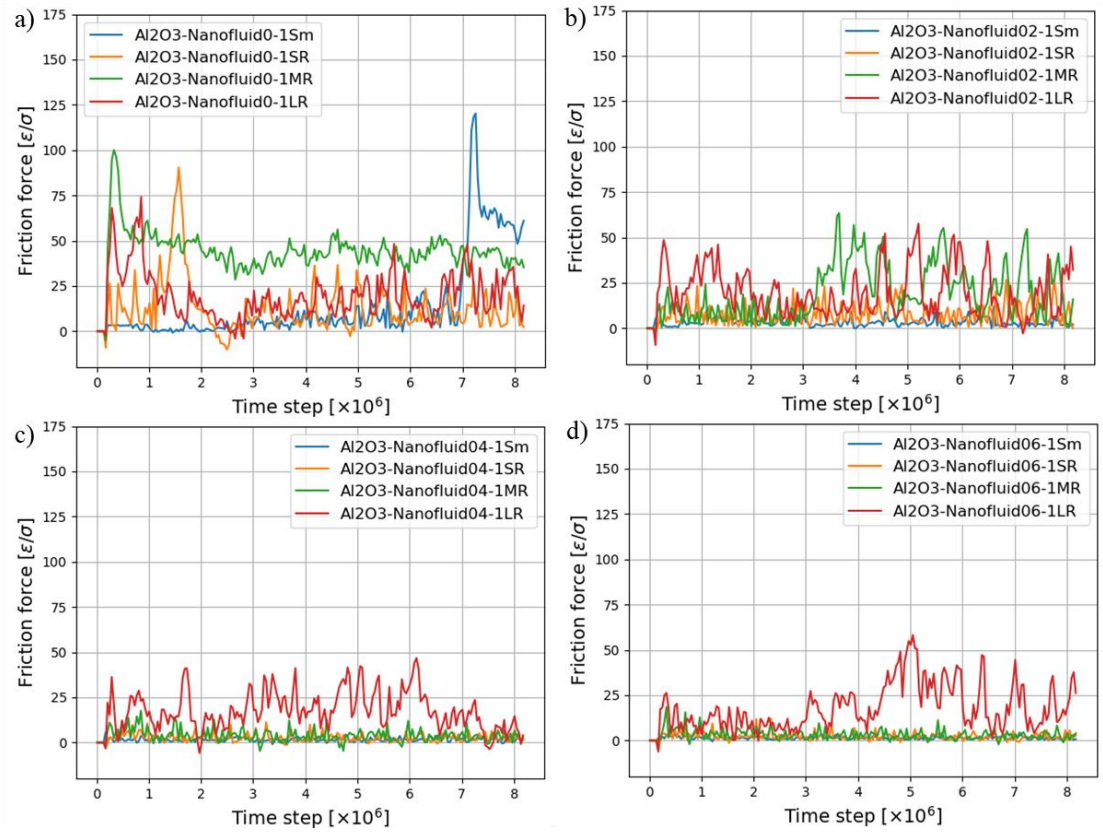

Figure 8 The friction force with respect to sliding time step for single Al_2O_3 particle nanofluid model with liquid with the thickness of (a) 0, (b) 2, (c) 4 and (d) 6 σ confined between smooth (Sm), small (SR), medium (MR) and large (LR) roughness solid surface

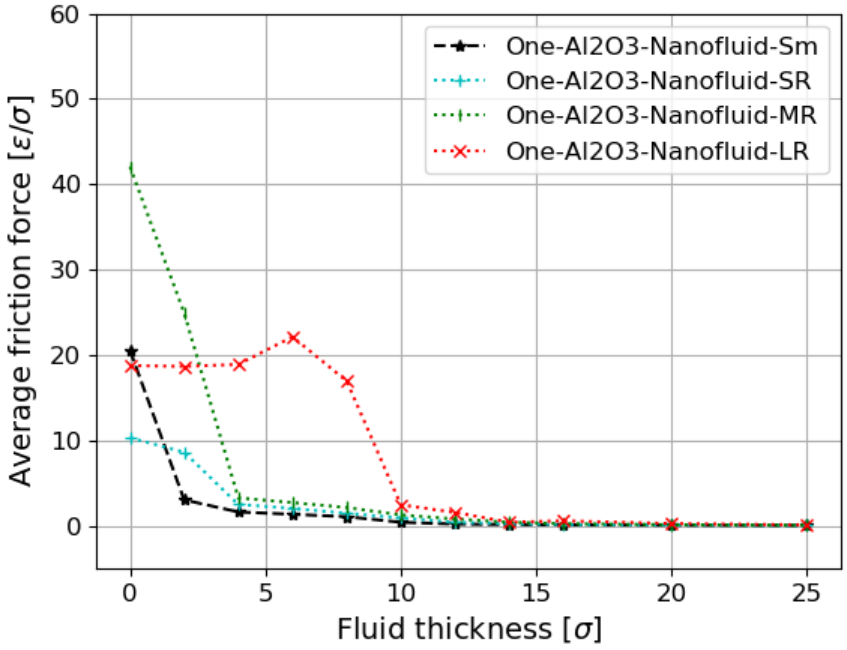

Figure 9 Friction force as a function of fluid thickness for single Al_2O_3 particle nanofluid model

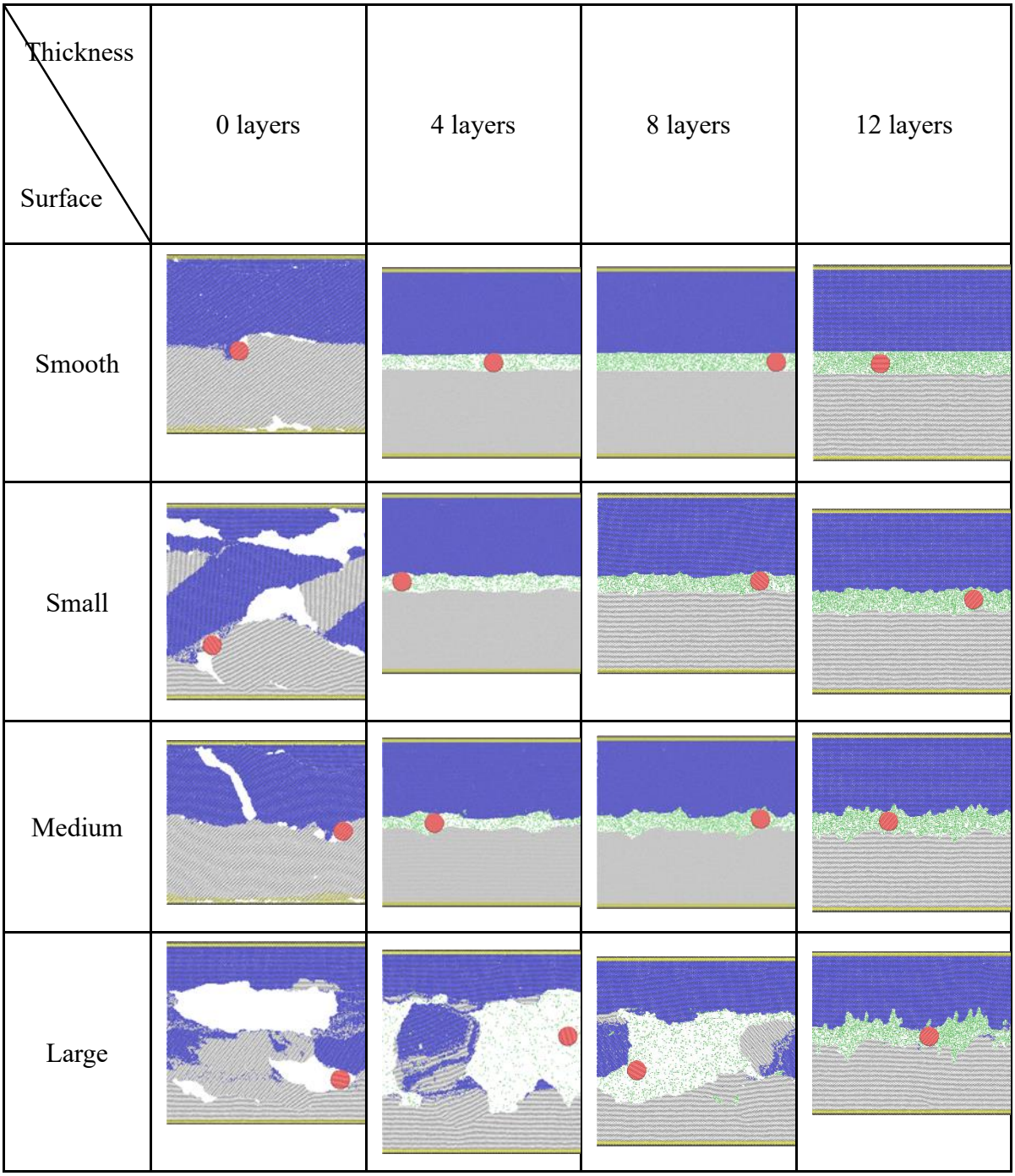

Figure 10 Final state images for single Al_2O_3 particle nanofluid model with liquid with the thickness of 0, 4, 8, 12 σ confined between smooth, small, medium, and large roughness solid surfaces

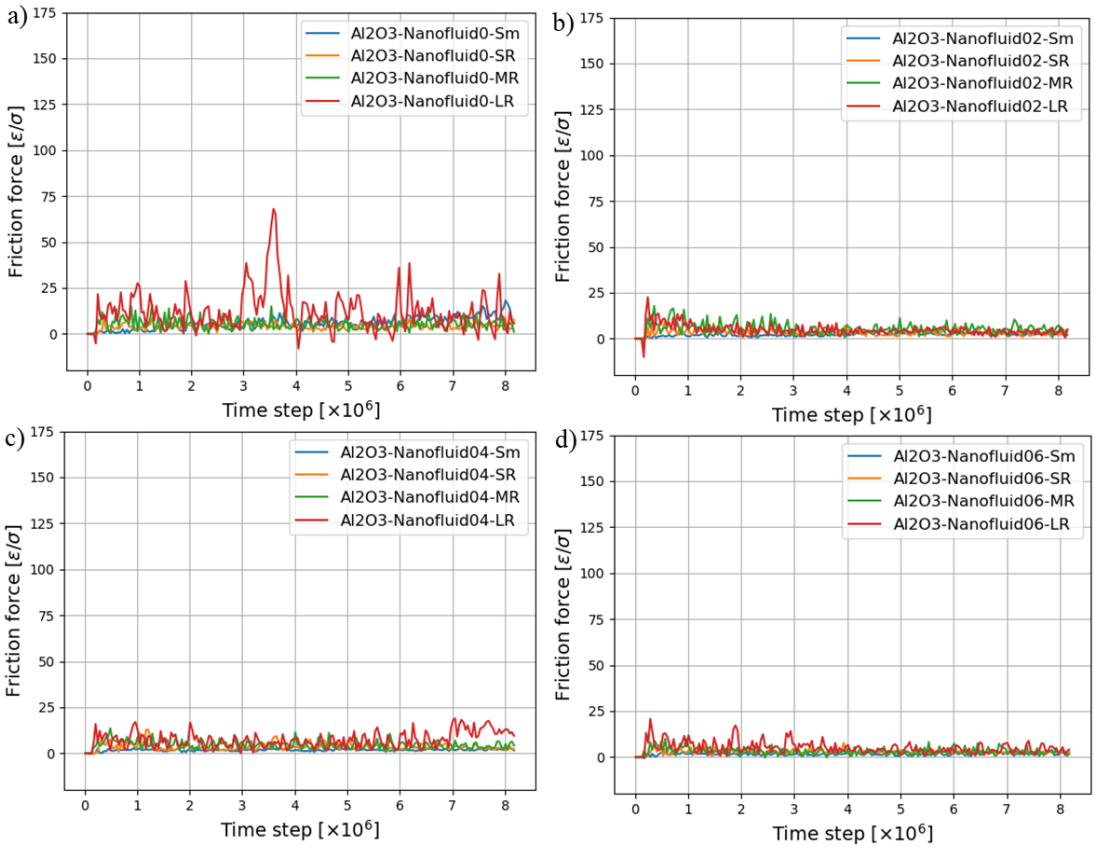

Figure 11 The friction force with respect to sliding time step for five Al_2O_3 particle nanofluid model with liquid with the thickness of (a) 0, (b) 2, (c) 4 and (d) 6 σ confined between smooth (Sm), small (SR), medium (MR) and large (LR) roughness solid surfaces

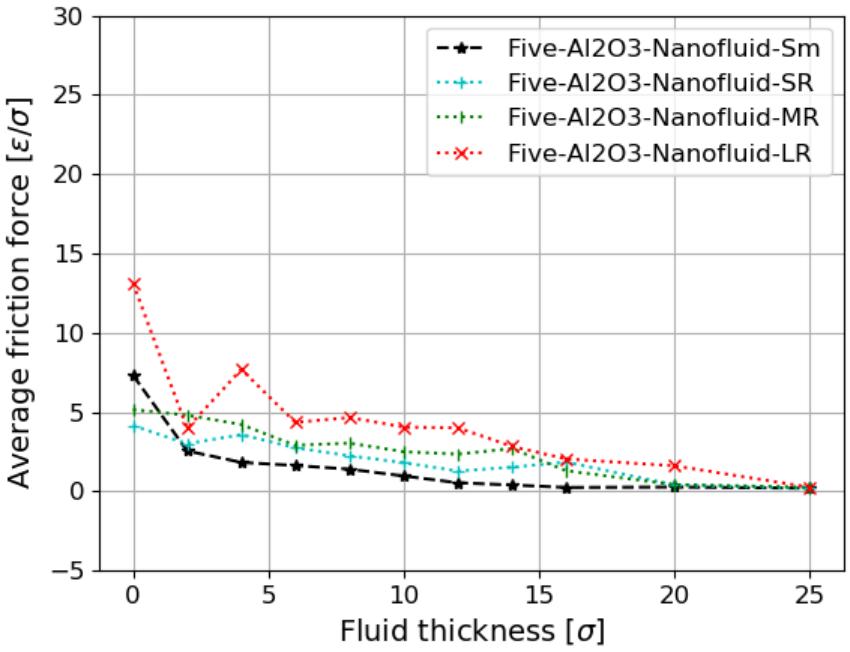

Figure 12 Friction force as a function of fluid thickness for five Al_2O_3 particle nanofluid model

Thickness / Surface	0 layers	4 layers	8 layers	12 layers
Smooth	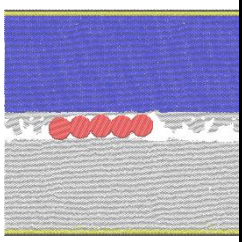	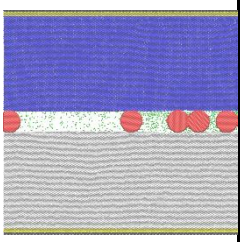	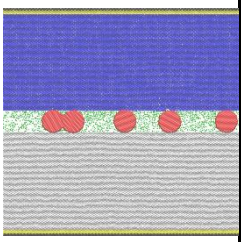	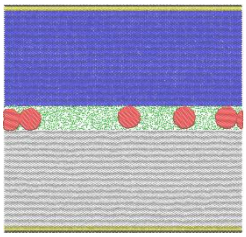
Small	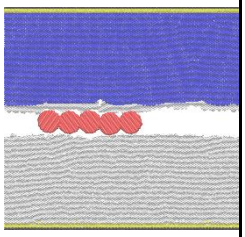	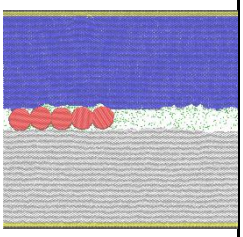	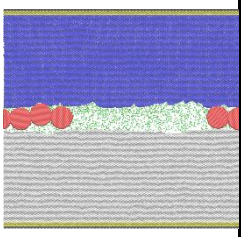	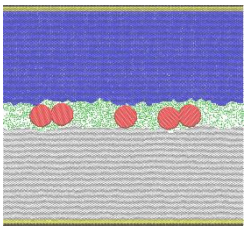
Medium	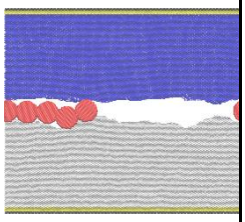	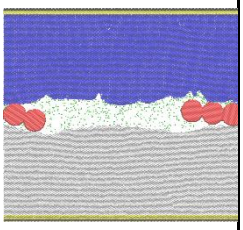	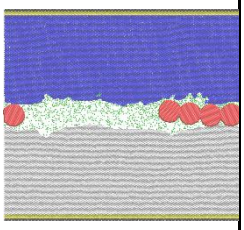	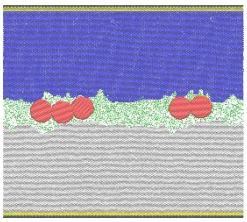
Large	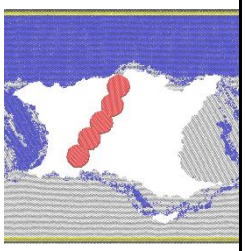	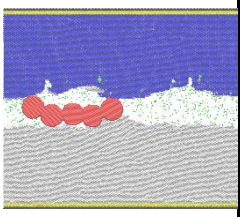	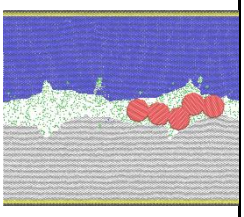	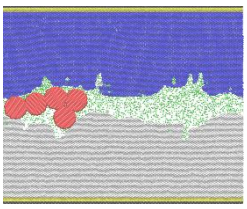

Figure 13 Final state images for five Al_2O_3 particle nanofluid model with liquid with the thickness of 0, 4, 8, 12 σ confined between smooth, small, medium, and large roughness solid surfaces

for multiple particle nanofluid models with liquid with the thickness of four, eight, and twelve units confined between smooth, small, medium, and large roughness surfaces. Nanoparticles tend to aggregate together and polish the rough surfaces during the sliding process. From all the simulation results, we can find that the friction force reduced greatly with models lubricated by nanofluid or base fluid compared to the dry friction model. In addition, the smoother the surface is, the greater the friction reduces, which supports the experimental finding of Gara and Zou [12].

4.2 Effect of nanoparticles

There were totally four types of nanoparticles with different hardness values, as shown in Table 4, Al_2O_3, ZrO_2, ZnO and CuO built with different characteristic energy values in this simulation were employed to investigate the effect of particle hardness on the tribological properties of nanofluids. The properties of Al_2O_3 nanofluid has been displayed in section 4.1.2 and 4.1.3, and we will discuss the effects of those left ZrO_2, ZnO and CuO nanofluids in this section.

4.2.1 Models with ZrO2 nanofluid

Being akin to section 4.1.2, models built with one ZrO_2 particle nanofluid confined between smooth (Sm), small (SR), medium (MR) and large (LR) roughness surfaces were studied. ZrO_2 particle has lower hardness than Al_2O_3 particle. Figure 14 shows the evolution of friction force with respect to sliding time step for the one ZrO_2 particle nanofluid for fluid thickness of zero, two, four, and six units, respectively.

Except for no fluid models, the smooth surface models with one particle nanofluid always shows the lowest friction force. When the fluid thickness is equal to or larger than 2σ, the friction force reduces as the roughness decreases, which can be seen from Figure 15. Visualization of the MD trajectories shows the particle separates the top and bottom surfaces for one particle nanofluid models with liquid with the thickness of four, eight, and twelve units confined between smooth, small, and medium roughness surfaces, as displayed in Figure 16.

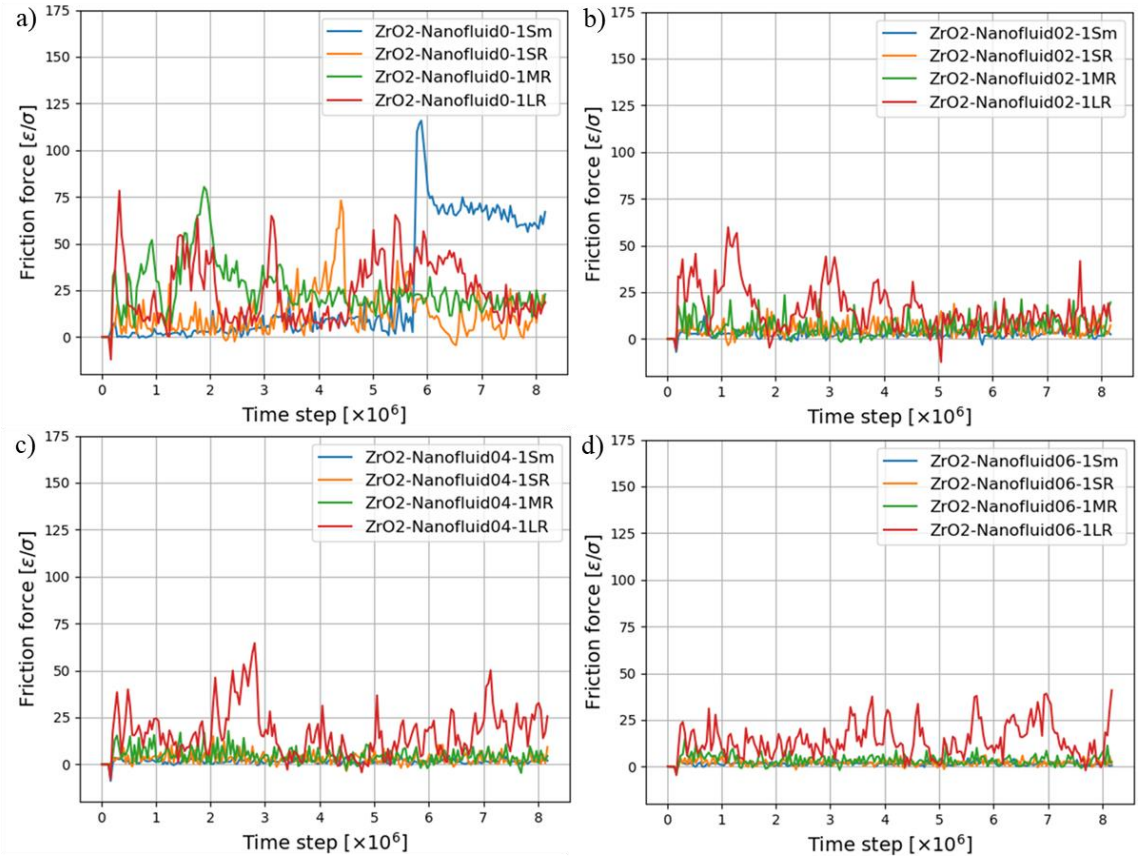

Figure 14 The friction force with respect to sliding time step for single ZrO_2 particle nanofluid model with liquid with the thickness of (a) 0, (b) 2, (c) 4 and (d) 6 σ confined between smooth (Sm), small (SR), medium (MR) and large (LR) roughness solid surfaces

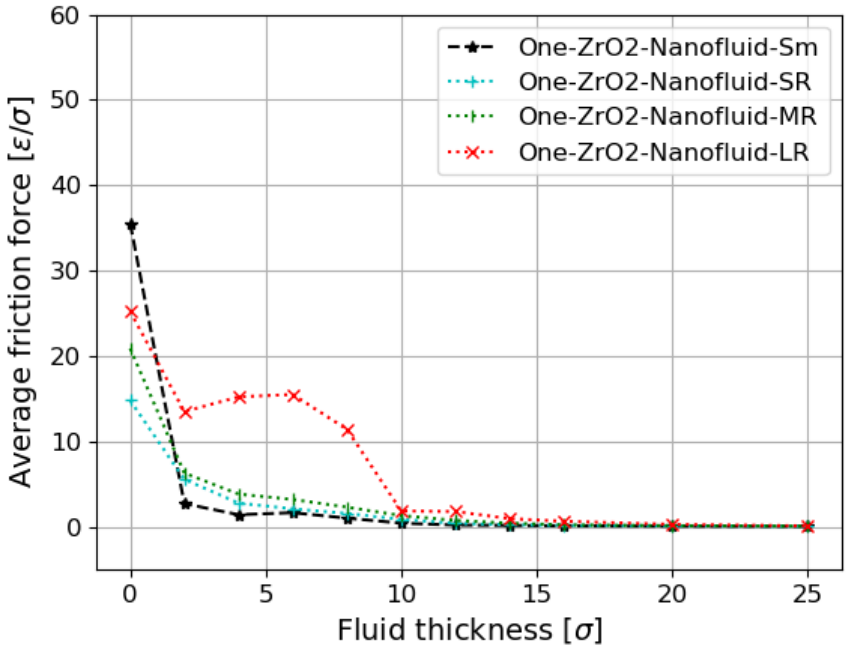

Figure 15 Friction force as a function of fluid thickness for single ZrO_2 particle nanofluid model

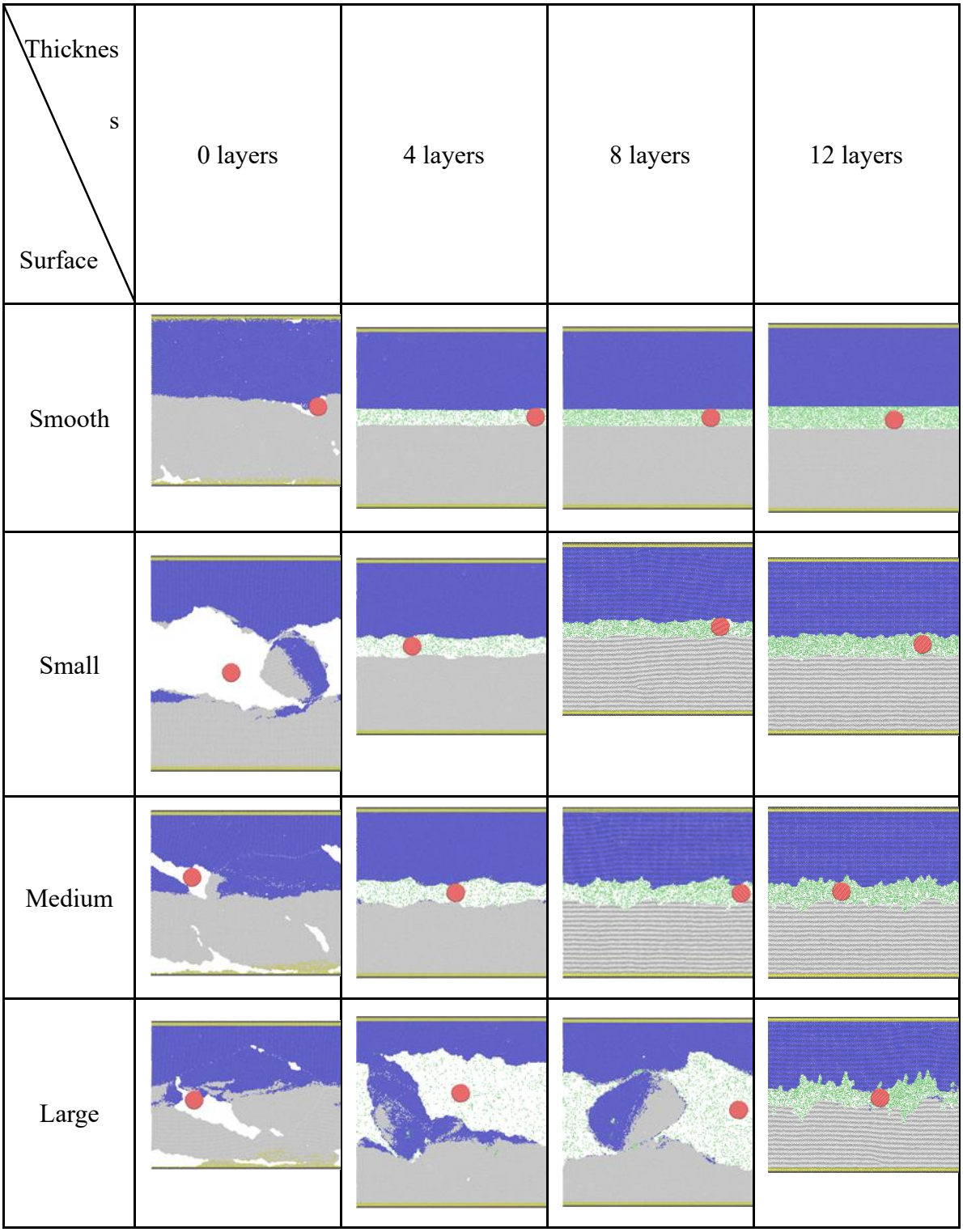

Figure 16 Final state images for single ZrO_2 particle nanofluid model with liquid with the thickness of 0, 4, 8, 12 σ confined between smooth, small, medium, and large roughness solid surfaces

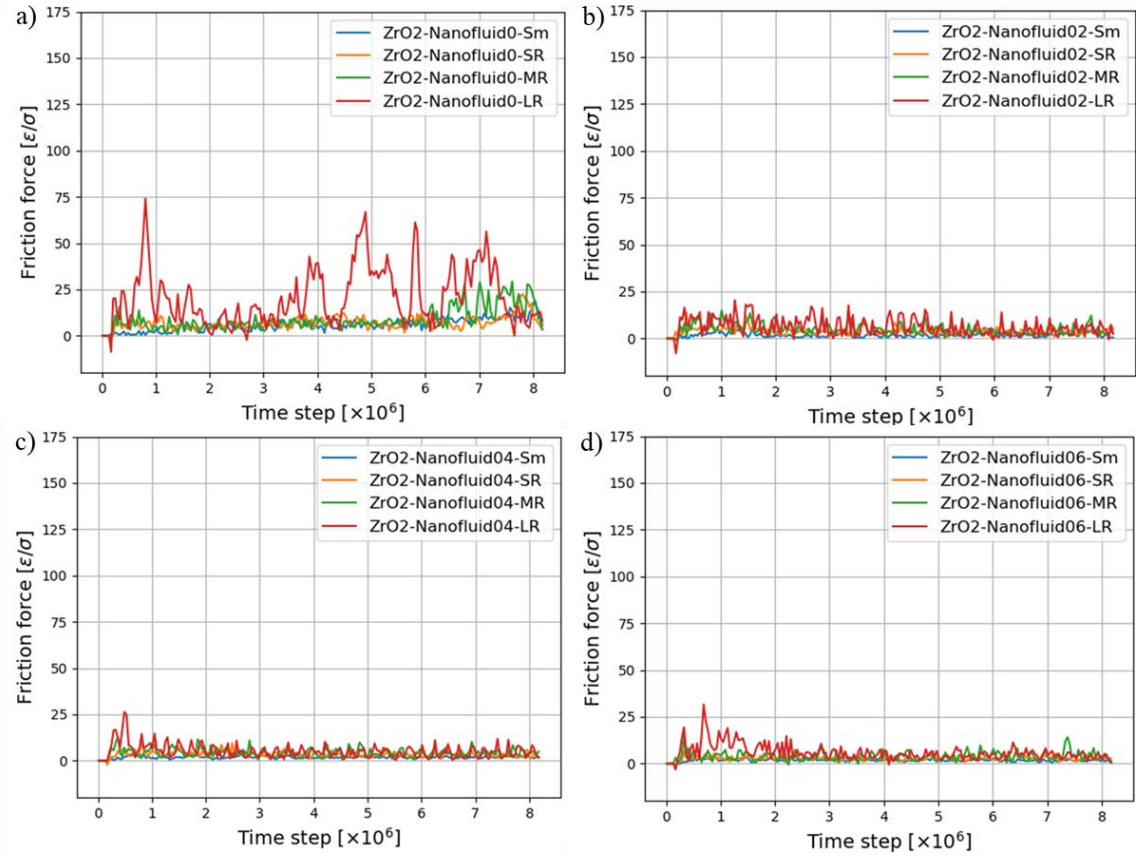

Figure 17 The friction force with respect to sliding time step for five ZrO_2 particle nanofluid model with liquid with the thickness of (a) 0, (b) 2, (c) 4 and (d) 6 σ confined between smooth (Sm), small (SR), medium (MR) and large (LR) roughness solid surfaces

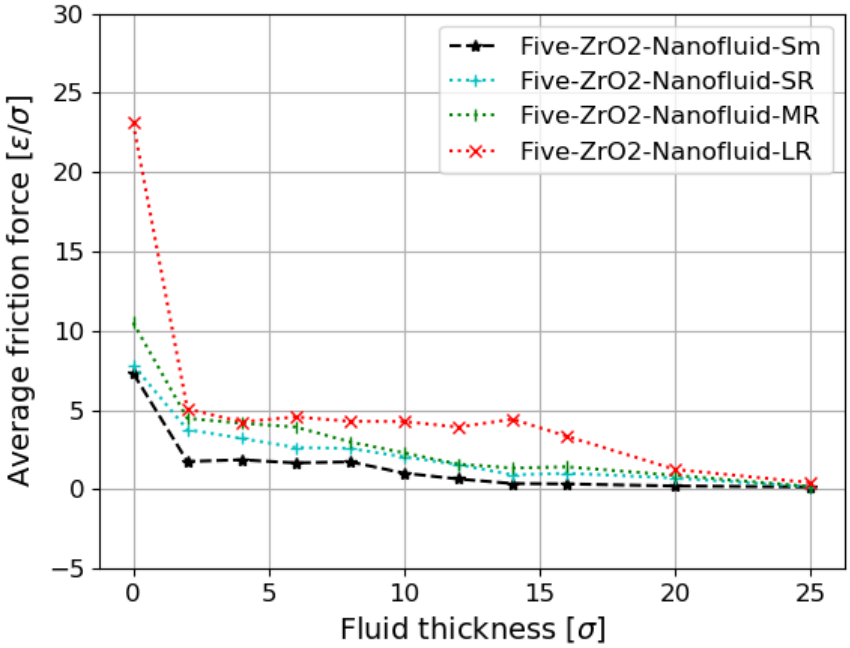

Figure 18 Friction force as a function of fluid thickness for five ZrO_2 particle nanofluid model

Thickness / Surface	0 layers	4 layers	8 layers	12 layers
Smooth	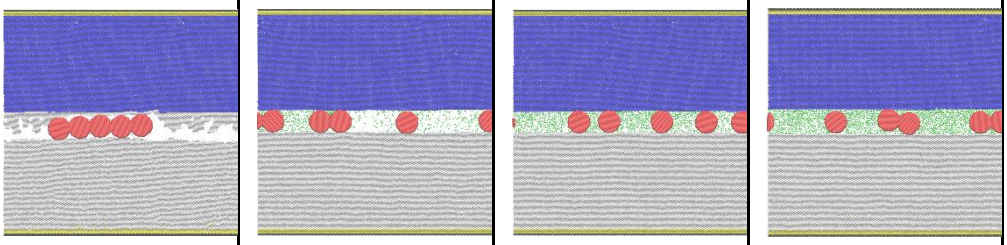			
Small	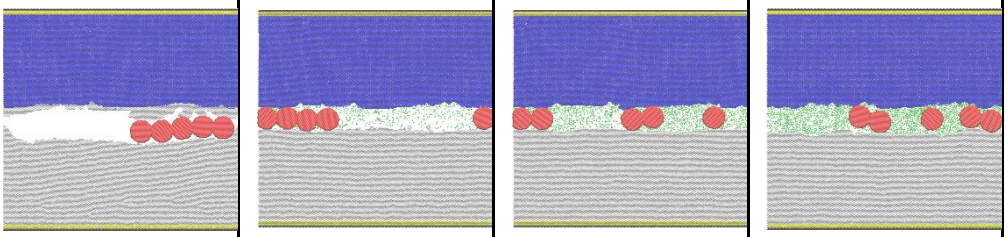			
Medium	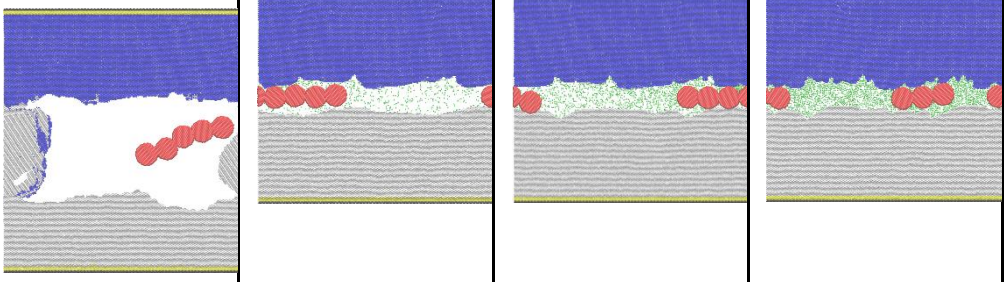			
Large	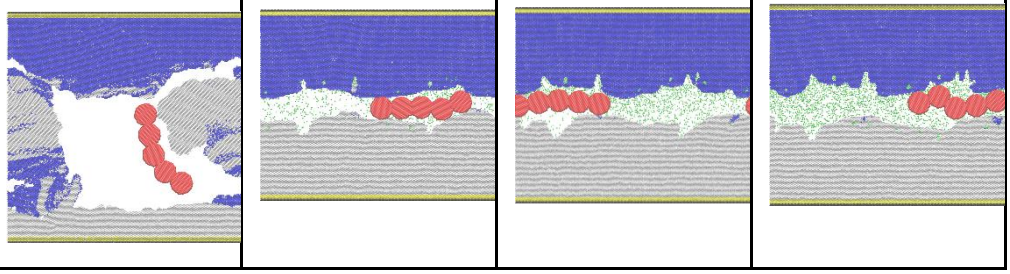			

Figure 19 Final state images for five ZrO_2 particle nanofluid model with liquid with the thickness of 0, 4, 8, 12 σ confined between smooth, small, medium, and large roughness solid surfaces

Being analogous to section 4.1.3, models built with multiple ZrO_2 particles nanofluid confined between smooth (Sm), small (SR), medium (MR) and large (LR) roughness surfaces were studied. Figure 17 shows the evolution of friction force with respect to sliding time step for the five particles nanofluid for fluid thickness of zero, two, four, and six units, respectively. Average friction force displayed in Figure 18 shows that the friction force of the smooth surface model is always lowest. Friction force increases when roughness increases. Visualization of the MD trajectories in Figure 19 shows that the particle separates the top and bottom surfaces for multiple particle nanofluid models with liquid with the thickness of four, eight, and twelve units confined between smooth, small, medium, and large roughness surfaces. Nanoparticles tend to aggregate together for models with rough surfaces during the sliding process.

4.2.2 Models with ZnO nanofluid

Being akin to section 4.2.1, models built with one ZnO particle nanofluid confined between smooth (Sm), small (SR), medium (MR) and large (LR) roughness surfaces were studied. Figure 20 shows the evolution of friction force with respect to sliding time step for the one ZnO particle nanofluid for fluid thickness of zero, two, four, and six units, respectively. The smooth surface models with one particle nanofluid always shows the lowest friction force. Except for no fluid models, the friction force reduces as the roughness decreases, which can be seen from Figure 21.

Visualization of the MD trajectories shows the particle separates the top and bottom surfaces for one particle nanofluid models with liquid with the thickness of four, eight, and twelve units confined between smooth, small, and medium roughness surfaces, as displayed in Figure 22.

Being analogous to section 4.2.1, models built with multiple ZnO particles nanofluid confined between smooth (Sm), small (SR), medium (MR) and large (LR) roughness surfaces were studied. Figure 23 shows the evolution of friction force with respect to sliding time step for the five particles nanofluid for fluid thickness of zero, two, four, and six units, respectively. Average friction force displayed in Figure 24 shows that the friction force of the smooth surface model is always lowest. As roughness increases, friction increases. Visualization of the MD trajectories in Figure 25 shows that the particle separates the top and bottom surfaces for multiple particle nanofluid models with liquid with the thickness of four, eight, and twelve units confined between smooth, small, medium, and large roughness surfaces. Nanoparticles tend to aggregate together and polish the rough surfaces during the sliding process.

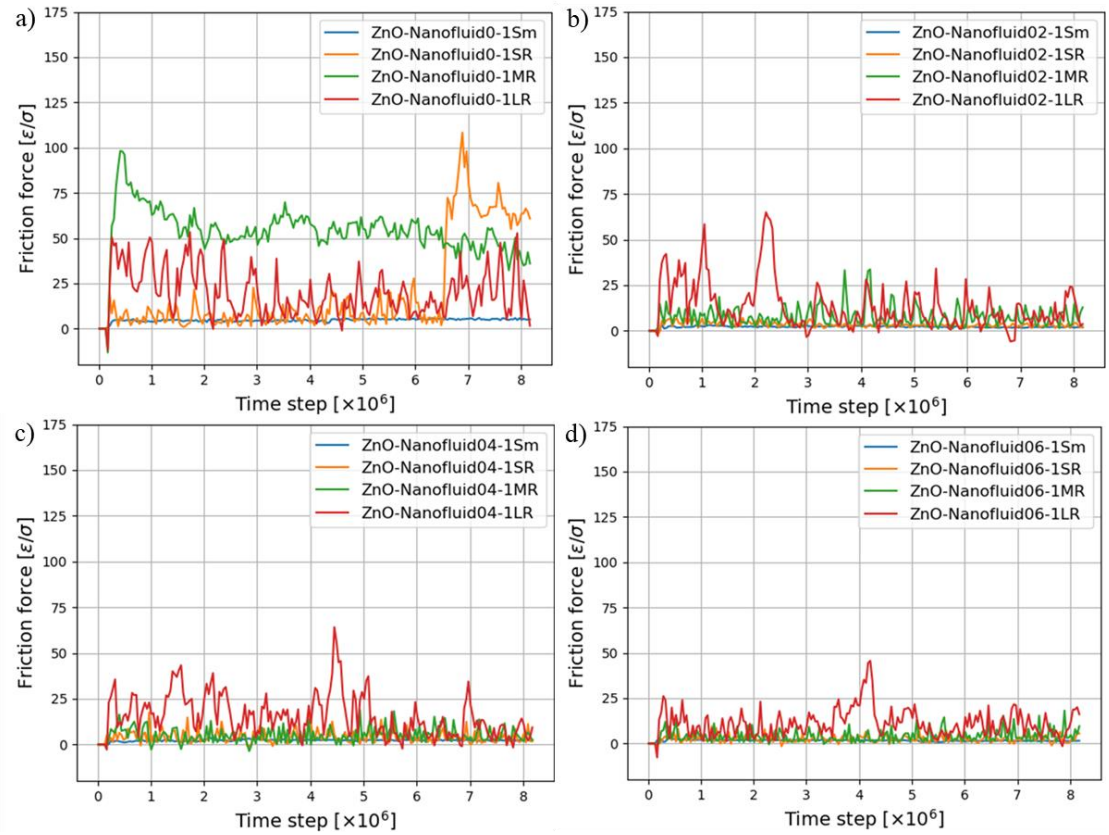

Figure 20 The friction force with respect to sliding time step for single ZnO particle nanofluid model with liquid with the thickness of (a) 0, (b) 2, (c) 4 and (d) 6 σ confined between smooth (Sm), small (SR), medium (MR) and large (LR) roughness solid surfaces

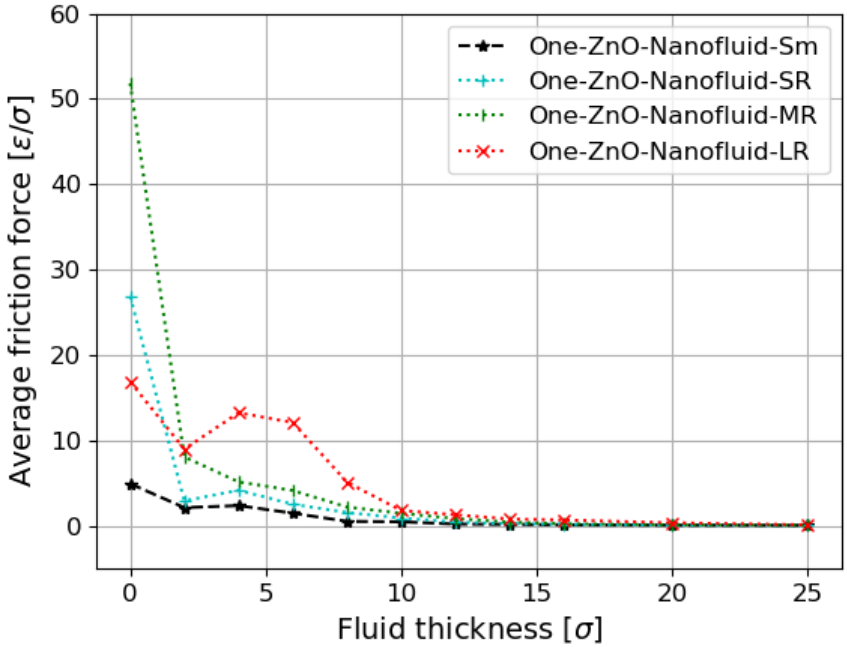

Figure 21 Friction force as a function of fluid thickness for single ZnO particle nanofluid model

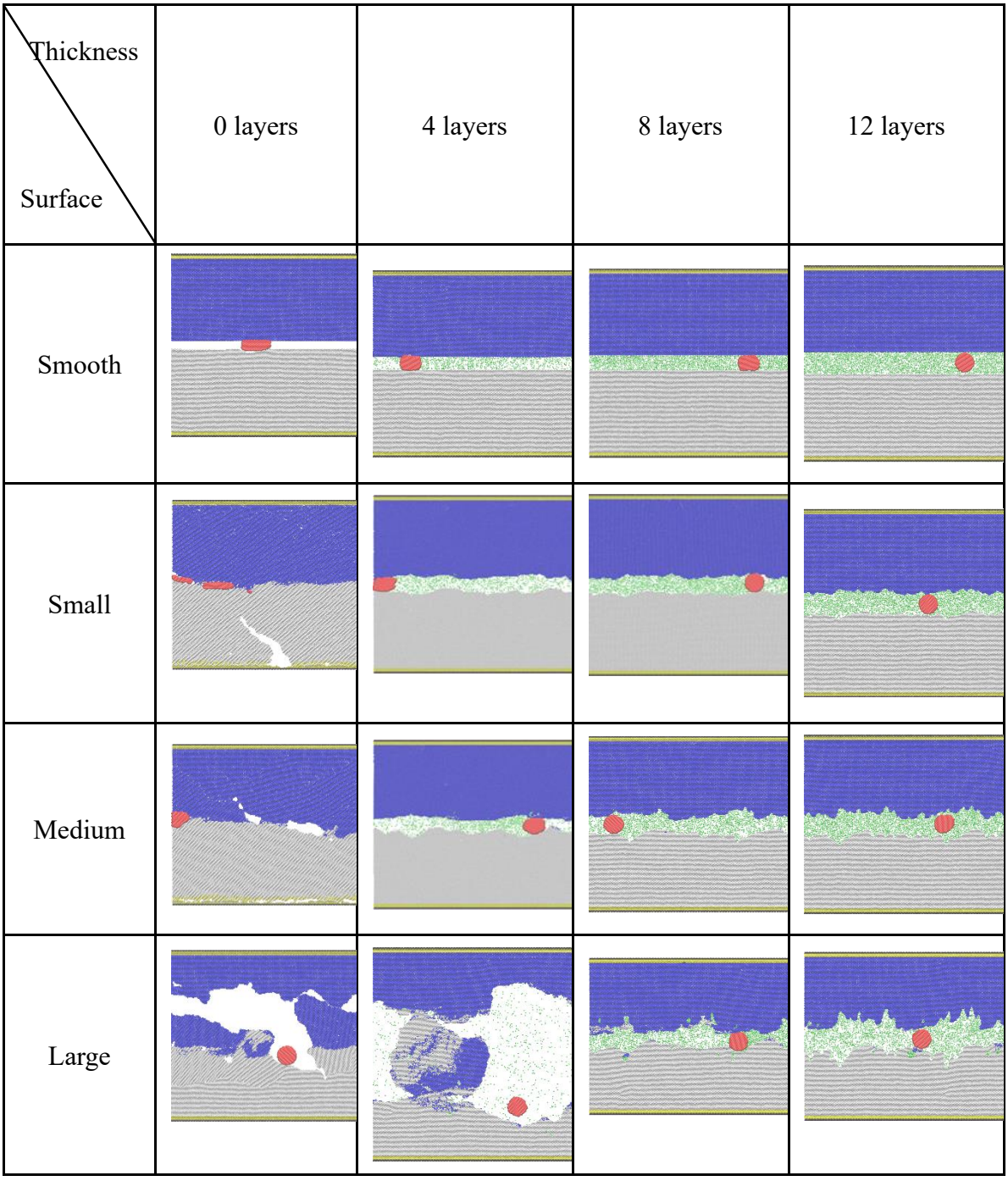

Figure 22 Final state images for one ZnO particle nanofluid model with liquid with the thickness of 0, 4, 8, 12 σ confined between smooth, small, medium, and large roughness solid surfaces

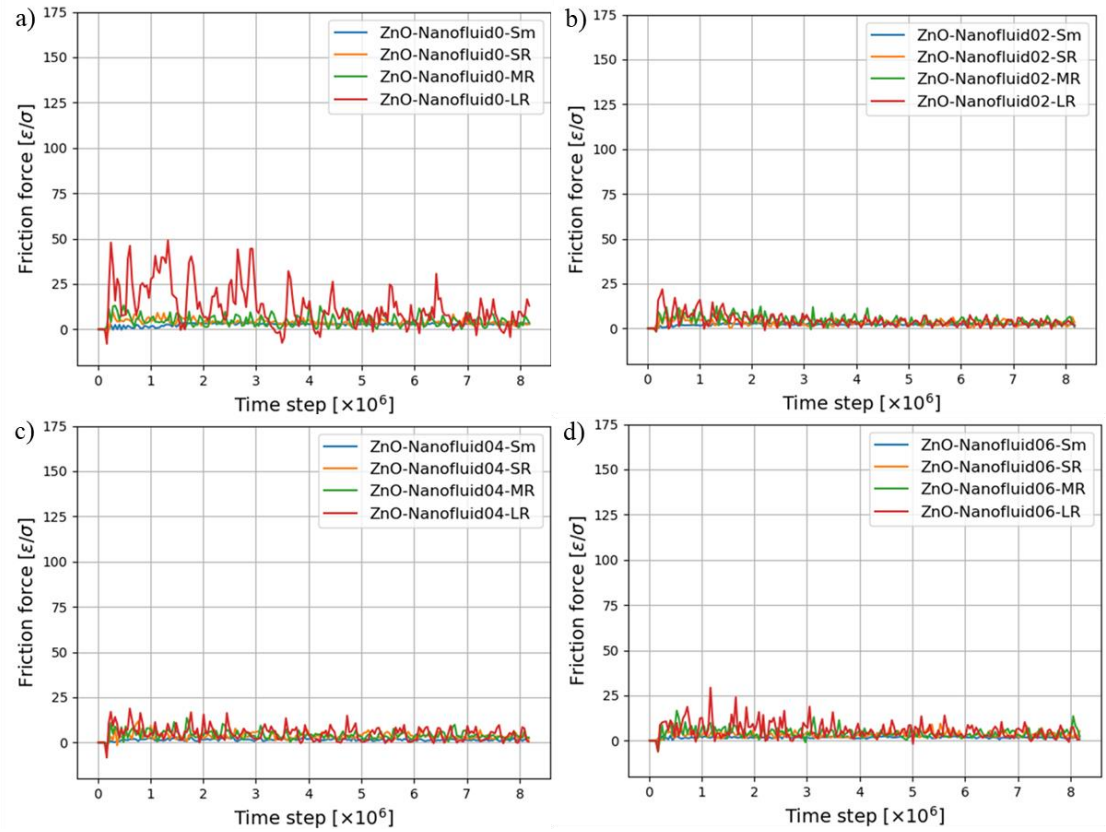

Figure 23 The friction force with respect to sliding time step for five ZnO particle nanofluid model with liquid with the thickness of (a) 0, (b) 2, (c) 4 and (d) 6 σ confined between smooth (Sm), small (SR), medium (MR) and large (LR) roughness solid surfaces

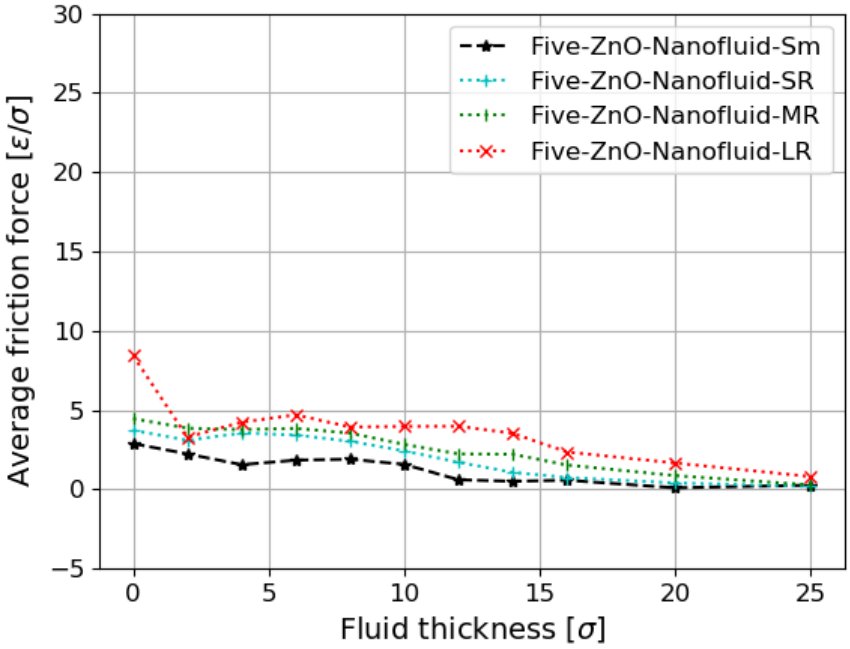

Figure 24 Friction force as a function of fluid thickness for five ZnO particle nanofluid model

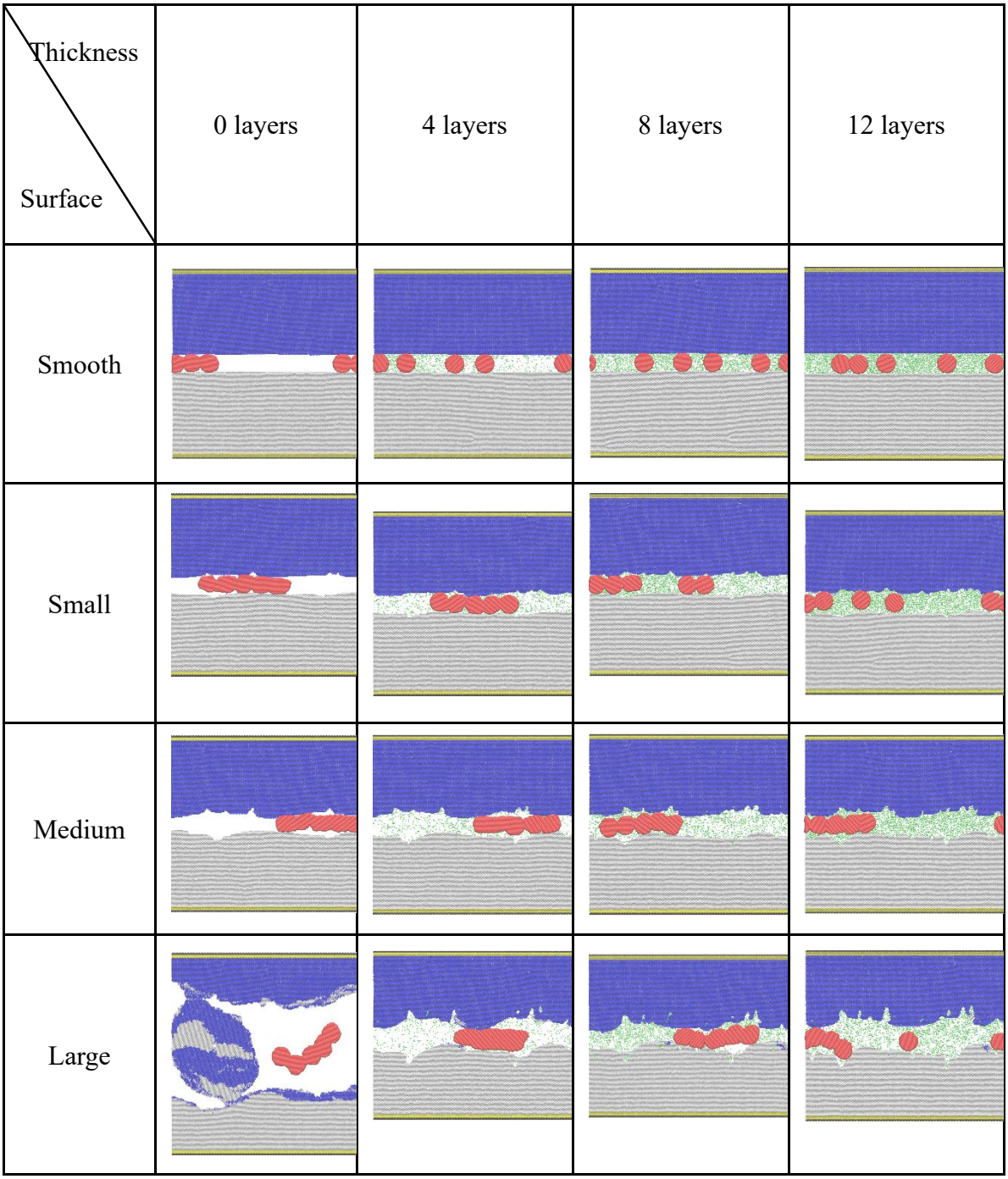

Figure 25 Final state images for five ZnO particle nanofluid model with liquid with the thickness of 0, 4, 8, 12 σ confined between smooth, small, medium, and large roughness solid surfaces

4.2.3 Models with CuO nanofluid

Being akin to section 4.2.1, models built with one CuO particle nanofluid confined between smooth (Sm), small (SR), medium (MR) and large (LR) roughness surfaces were studied. Figure 26 shows the evolution of friction force with respect to sliding time step for the one CuO particle nanofluid for fluid thickness of zero, two, four, and six units, respectively. The smooth surface models with one particle nanofluid always shows the lowest friction force. When the fluid thickness is larger than 2σ, the friction force reduces as the roughness decreases, which can be seen from Figure 27. Visualization of the MD trajectories shows the particle separates the top and bottom surfaces for one particle nanofluid models with liquid with the thickness of four, eight, and twelve units confined between smooth, small, and medium roughness surfaces, as displayed in Figure 28.

Being analogous to section 4.1.3, models built with multiple CuO particles nanofluid confined between smooth (Sm), small (SR), medium (MR) and large (LR) roughness surfaces were studied. Figure 29 shows the evolution of friction force with respect to sliding time step for the five particles nanofluid for fluid thickness of zero, two, four, and six units, respectively. Average friction force displayed in Figure 30 shows that the friction force of the smooth surface model is always lowest for all different rough models. As roughness increases, friction increases. Visualization of the MD trajectories in Figure 31 shows that the particle separates the top and bottom

surfaces for multiple particle nanofluid models with liquid with the thickness of four, eight, and twelve units confined between smooth, small, medium, and large roughness surfaces. Nanoparticles tend to aggregate together and crush on the rough surfaces during the sliding process.

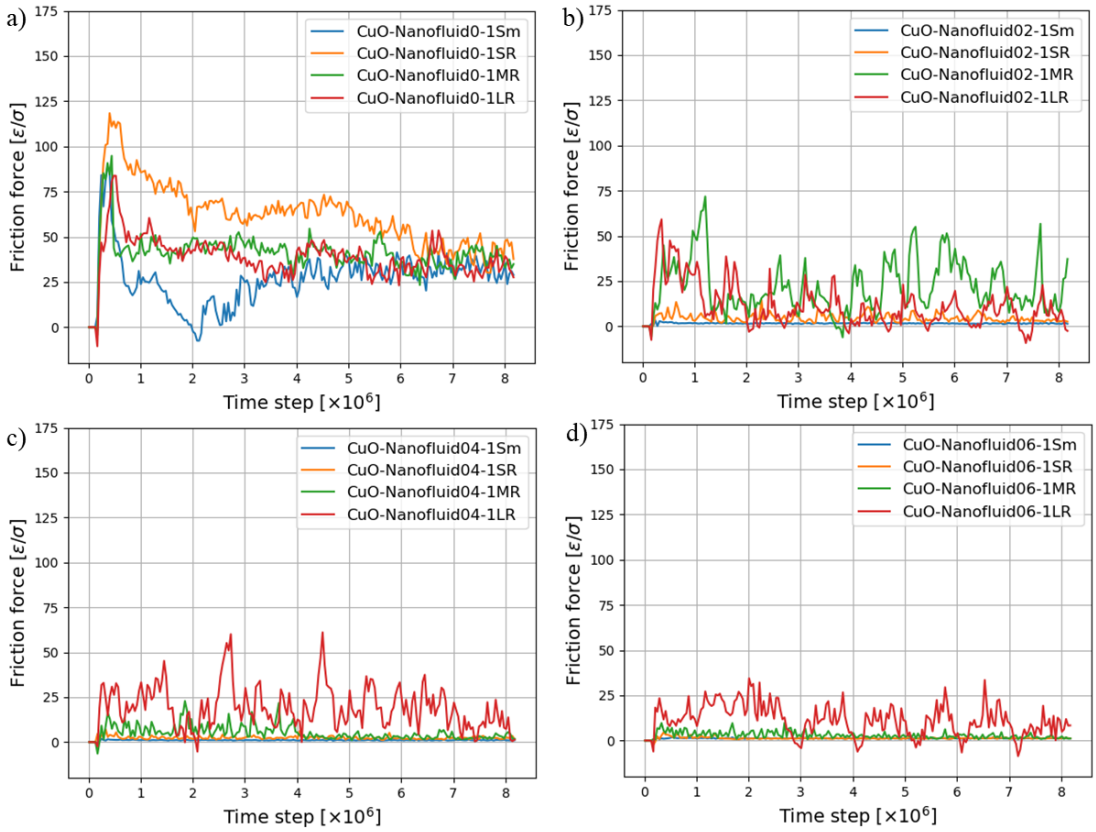

Figure 26 The friction force with respect to sliding time step for single CuO particle nanofluid model with liquid with the thickness of (a) 0, (b) 2, (c) 4 and (d) 6 σ confined between smooth (Sm), small (SR), medium (MR) and large (LR) roughness solid surfaces

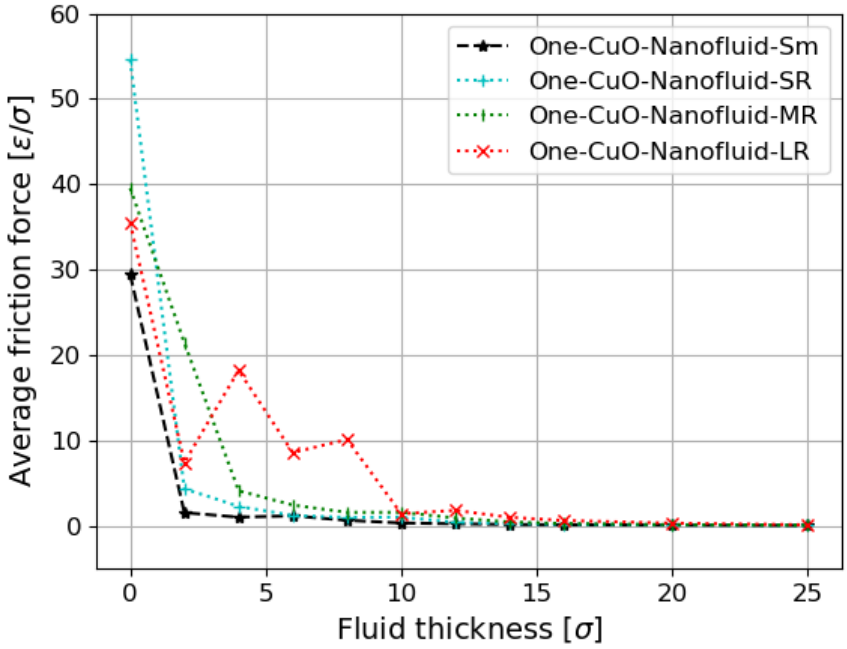

Figure 27 Friction force as a function of fluid thickness for single CuO particle nanofluid model

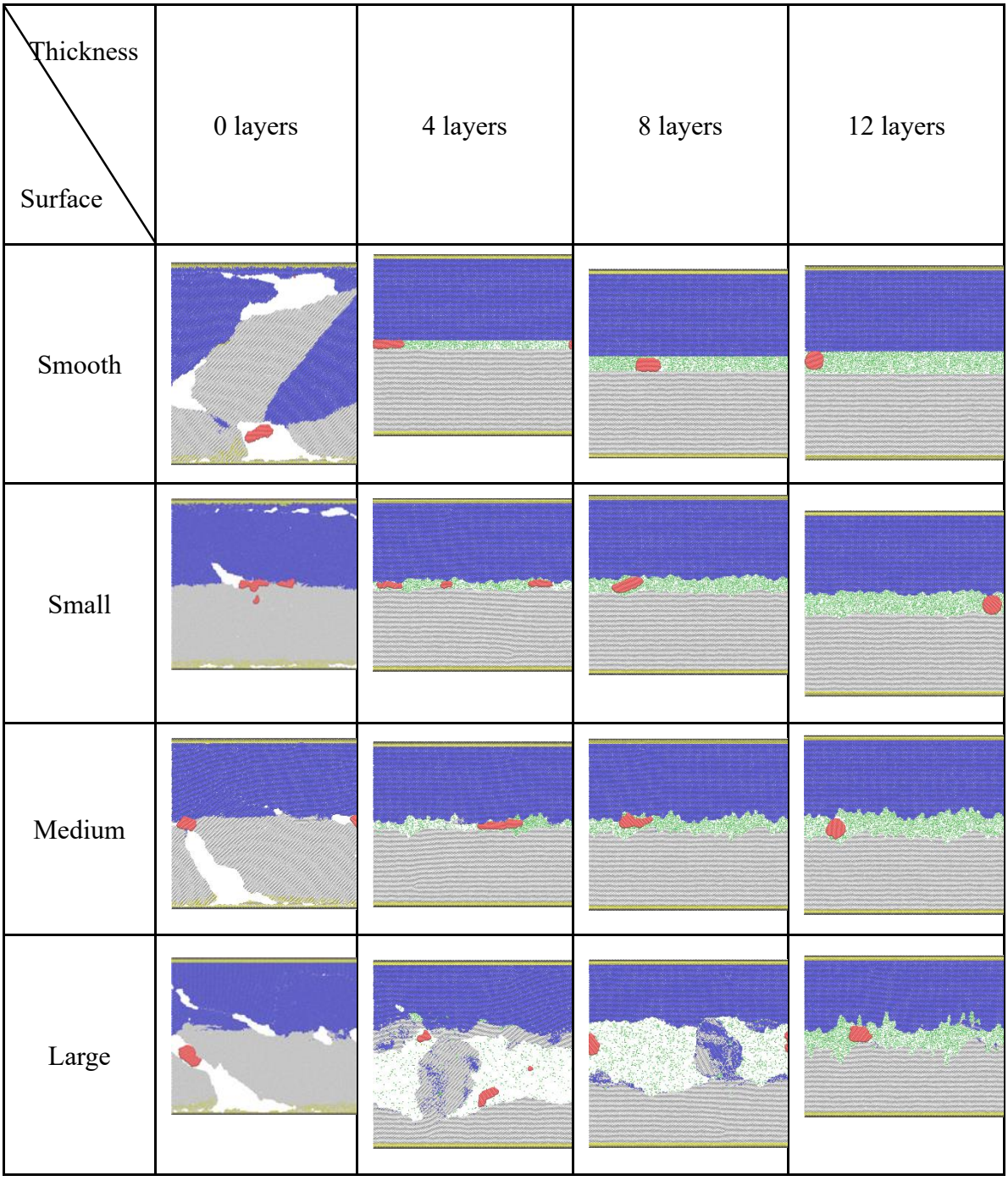

Figure 28 Final state images for single CuO particle nanofluid model with liquid with the thickness of 0, 4, 8, 12 σ confined between smooth, small, medium, and large roughness solid surfaces

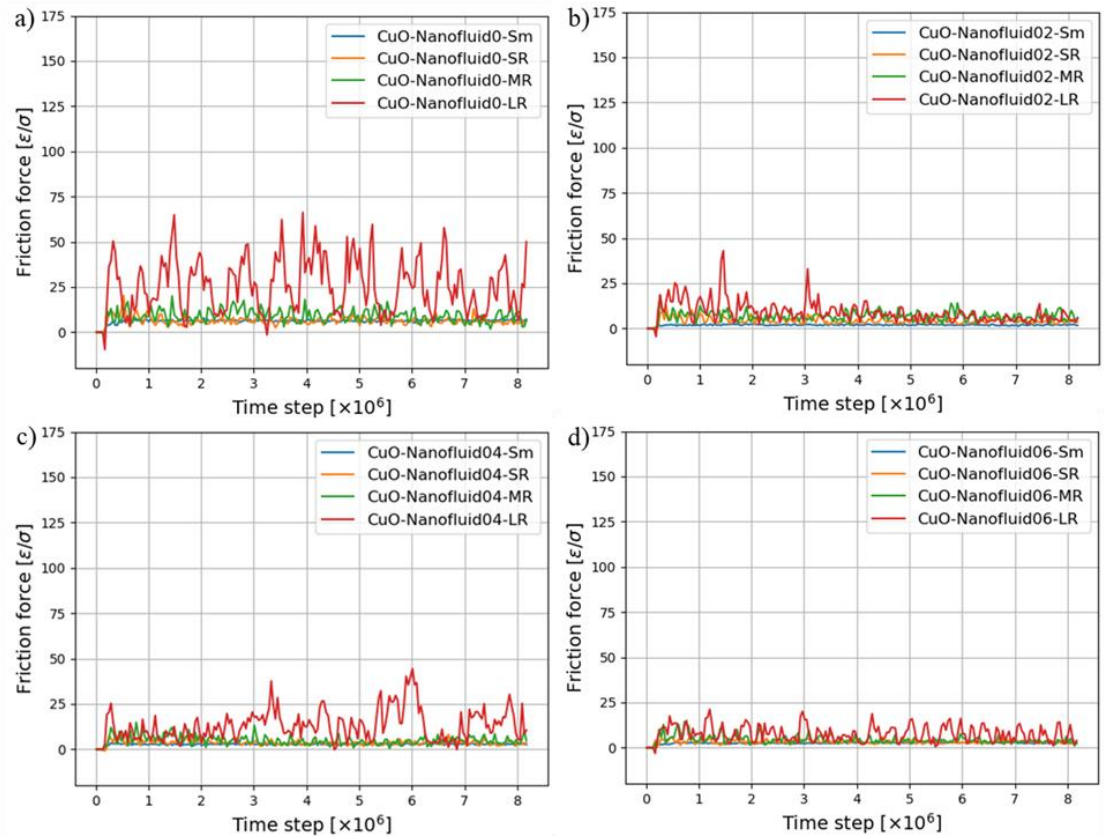

Figure 29 The friction force with respect to sliding time step for five CuO particle nanofluid model with liquid with the thickness of (a) 0, (b) 2, (c) 4 and (d) 6 σ confined between smooth (Sm), small (SR), medium (MR) and large (LR) roughness solid surfaces

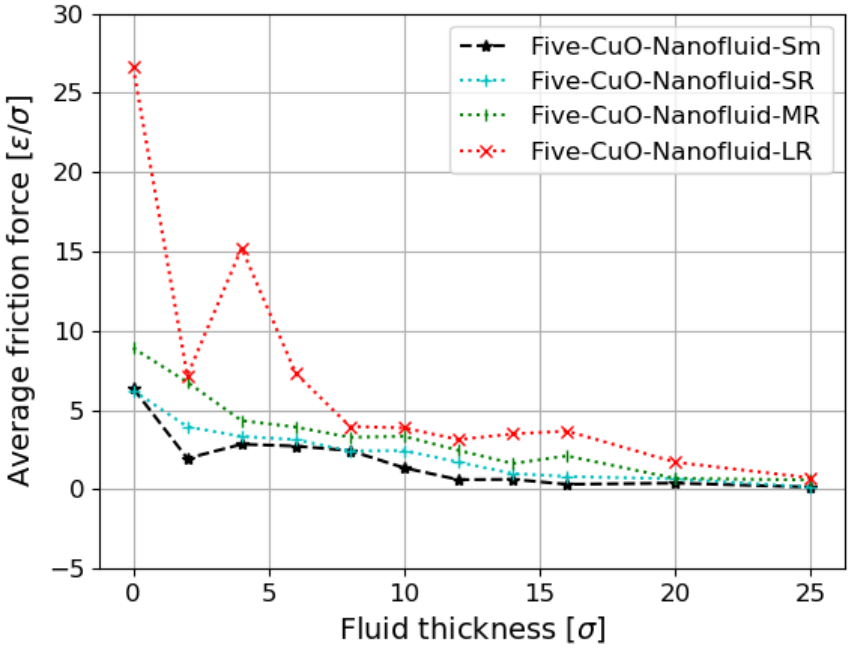

Figure 30 Friction force as a function of fluid thickness for five CuO particle nanofluid model

Thickness / Surface	0 layers	4 layers	8 layers	12 layers
Smooth	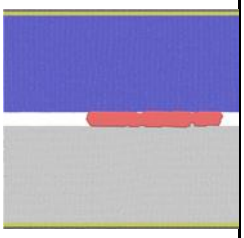	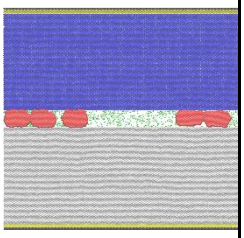	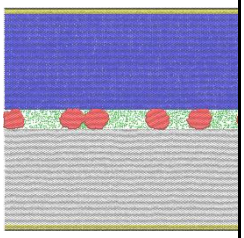	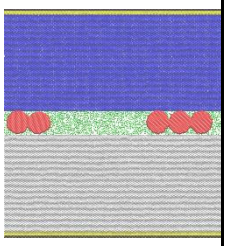
Small	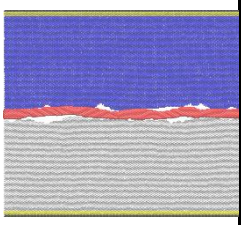	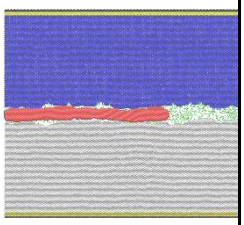	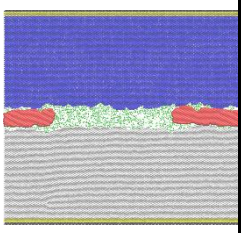	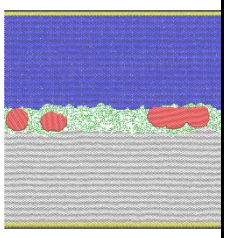
Medium	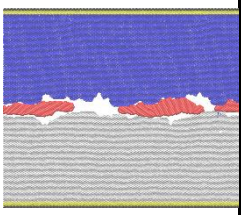	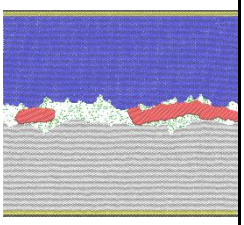	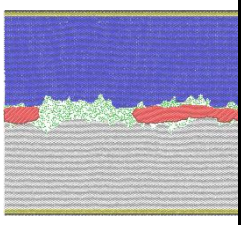	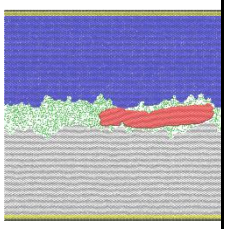
Large	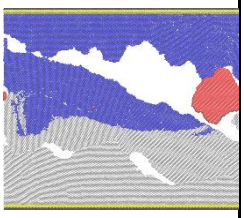	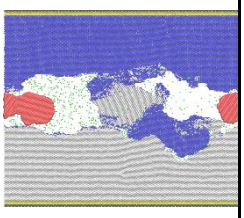	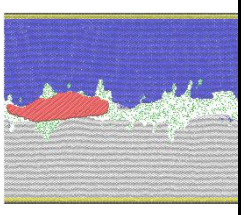	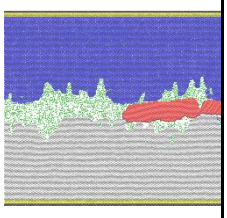

Figure 31 Final state images for five CuO particle nanofluid model with liquid with the thickness of 0, 4, 8, 12 σ confined between smooth, small, medium, and large roughness solid surfaces

4.3 Effect of fluid thickness

There are eleven initial lubricant fluid thickness: 0, 2, 4, 6, 8, 10, 12, 14, 16, 20 and 25 σ for 220 different simulation models with different solid surface roughness. In this section, we are going to investigate the influence of the thickness of the liquid and try to find out the reason.

4.3.1 Nanofluid models with different thickness of nanofluid

As displayed by Figure 6, the average friction force drops significantly when a fluid is introduced into the interface and the role of roughness is reserved. The significant wear and smoothing of the asperities, followed by fusion of the surfaces shown in Figure 7 explains why the models with no fluid show the highest friction force in all the models with four different roughness. What's more, in the rough surface models transfer films were formed during dry contact.

As fluid thickness increases, the average friction force for all levels of roughness converges from different critical fluid thickness value, which can be concluded from Figure 9, 15, 21 & 27 for single particle nanofluid models and Figure 12, 18, 24 & 30 for multiple particle nanofluid models. The critical fluid thickness values of single particle nanofluid models are 2σ for ZrO_2 and 4σ for Al_2O_3, ZnO & CuO nanofluid models. The critical fluid thickness values of multiple particle nanofluid models are 2σ for ZrO_2 & CuO and 4σ for Al_2O_3 & ZnO nanofluid models.

Final friction morphologies displayed in Figure 10, Figure 16, Figure 22 &

Figure 28 show that for the one particle nanofluid models with no fluid, the particle separates the smooth surfaces from the beginning of sliding and then the particle is stuck in a valley of the bottom surface of the smooth surface model. The MD trajectories in Figure 13, Figure 19 Figure 25 & Figure 31 shows that the particles separate the solid surfaces and tend to aggregate together and polish the rough surfaces during the sliding process. The aggregating nanoparticles reduce the contact of two solid surfaces by serving as a supporting effect for the surfaces, which supports the findings of Lv et al. [38] which showed supporting efforts from reunited Cu nanoparticles.

4.3.2 Nanofluid models with different types of nanoparticles

The influence of nanoparticles' type was studied by comparing the average friction force of base fluid and different nanofluid models confined by different roughness surfaces separately, as shown in Figure 32 to Figure 35. From Figure 32 we can see that single ZnO nanofluid model has the lowest average force for smooth, small and large rough surface models before the converge happens as fluid thickness increases. However, medium rough surface models lubricated with single ZrO_2 nanofluid exhibit the lowest friction force. The final state images displayed in Figure 33 reveal that smooth, small and large rough surface models confined ZnO nanofluid have the smoothest surfaces while medium rough surface models confined ZrO_2 nanofluid shows the smoothest surface.

Models confined by multiple ZnO nanofluid always exhibit the lowest friction force for all models with different roughness before the converging happens with increased fluid thickness, as shown in Figure 34. Visualization of the MD trajectories displayed in Figure 35 shows aggregation phenomenon within nanoparticles and these united nanoparticles tend to transfer together. ZnO and CuO particles crushed and united together to form a film between the top and bottom surfaces. From Table 4 we know that except particle CuO, Al_2O_3, ZrO_2 and ZnO particles have higher hardness than the solid steel surface. Within these three kinds of particles, ZnO particle has the most similar hardness value when compared with the hardness of the solid surfaces.

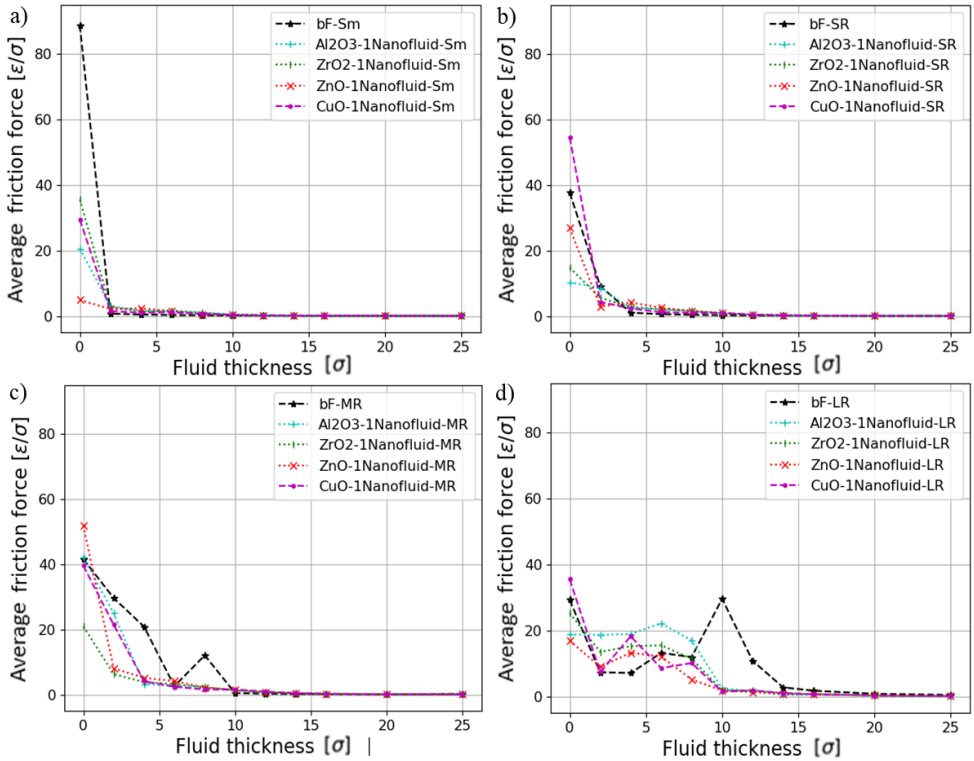

Figure 32 Average friction force for base fluid and single particle nanofluid models confined between smooth (Sm), small (SR), medium (MR) and large (LR) roughness solid surfaces

Particle / Surface Thickness	Al_2O_3	ZrO_2	ZnO	CuO
Smooth 2 layers	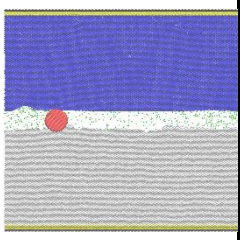	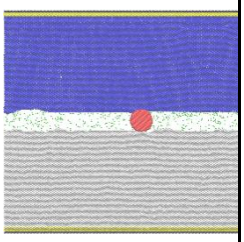	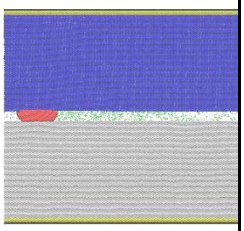	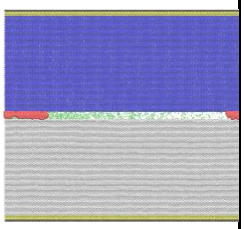
Small 2 layers	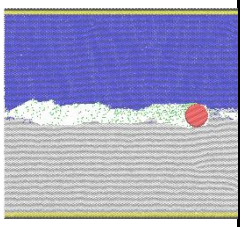	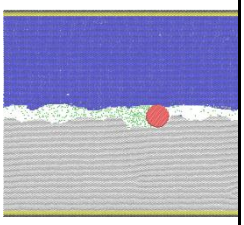	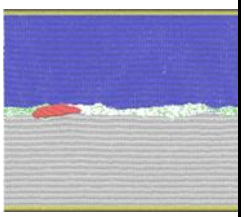	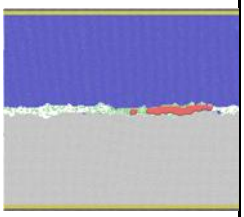
Medium 2 layers	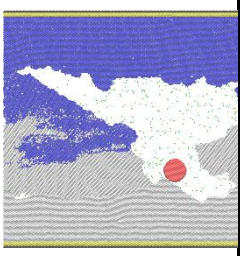	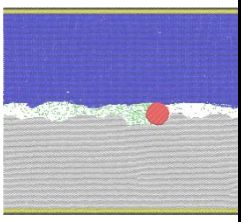	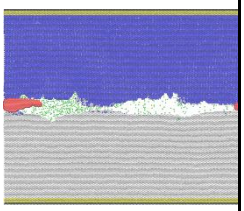	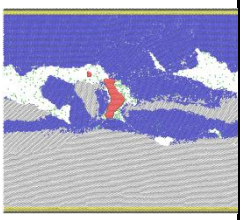
Large 8 layers	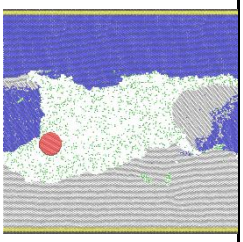	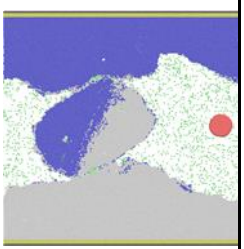	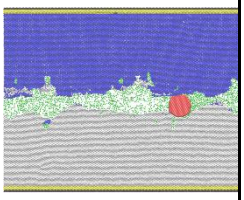	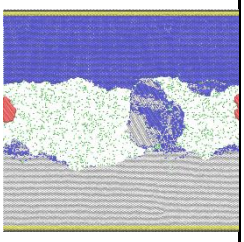

Figure 33 Final state images for single Al_2O_3, ZrO_2, ZnO and CuO nanofluid models with liquid thickness before converging confined between smooth, small, medium, and large roughness solid surfaces

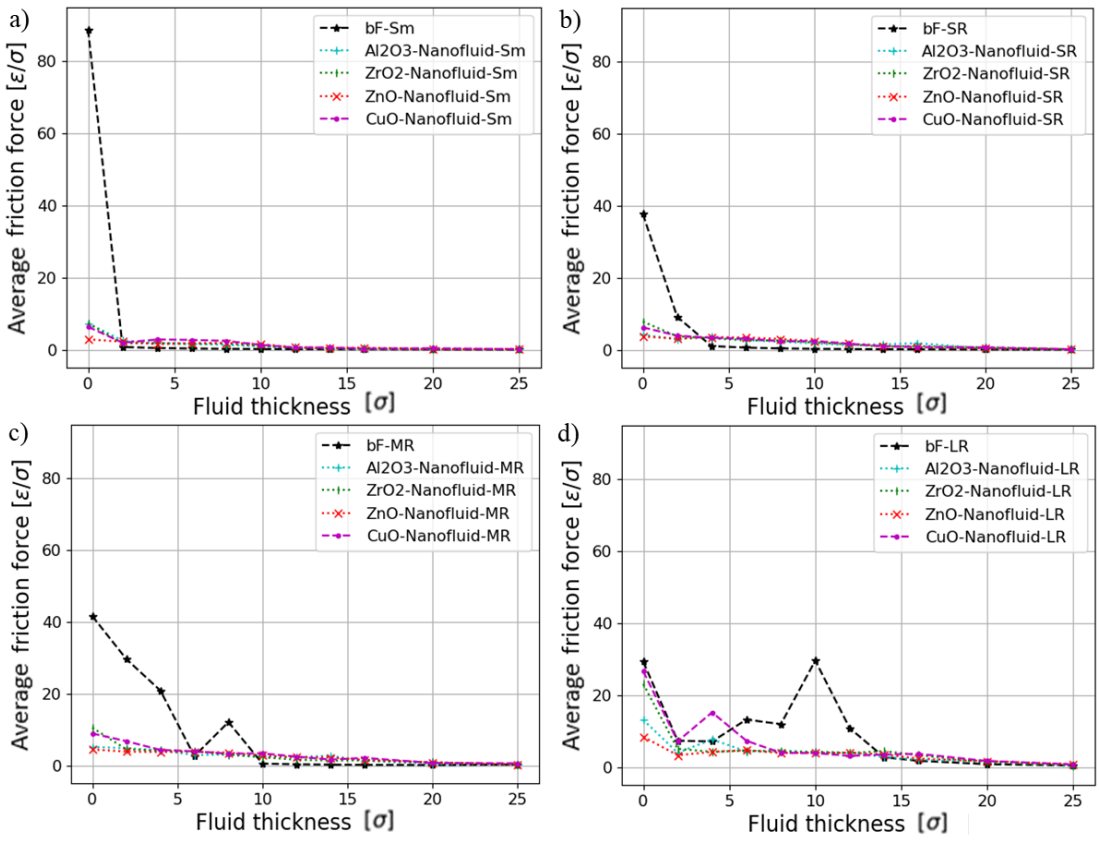

Figure 34 Average friction force for base fluid and multiple particles nanofluid models confined between smooth (Sm), small (SR), medium (MR) and large (LR) roughness solid surfaces

Particle / Surface Thickness	Al_2O_3	ZrO_2	ZnO	CuO
Smooth 2 layers	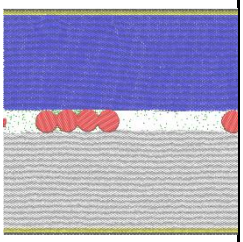	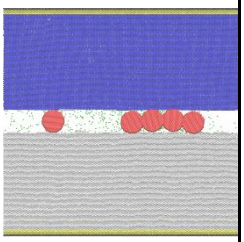	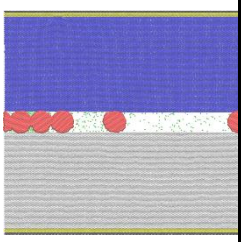	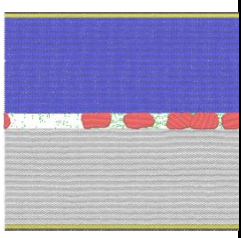
Small 2 layers	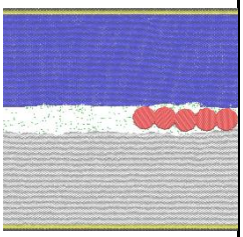	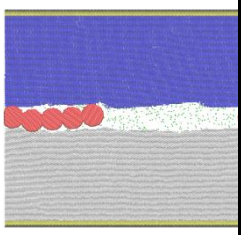	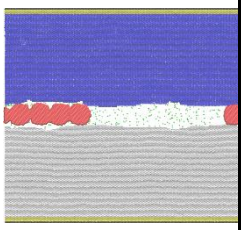	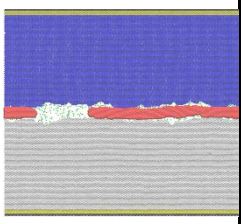
Medium 2 layers	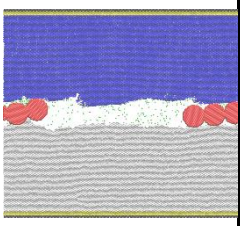	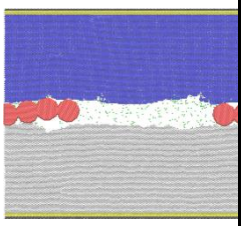	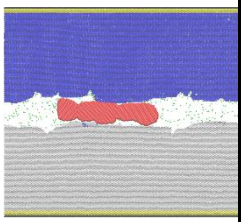	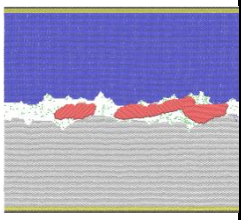
Large 2 layers	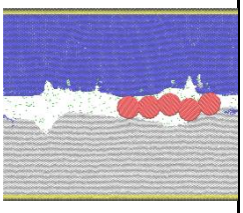	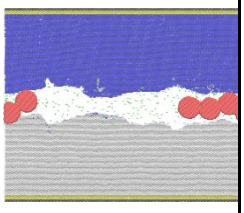	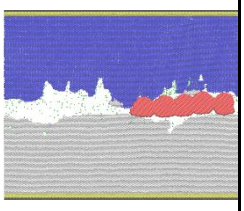	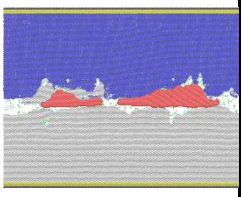

Figure 35 Final state images for multiple Al_2O_3, ZrO_2, ZnO and CuO nanofluid models with liquid thickness before converging confined between smooth, small, medium, and large roughness solid surfaces

4.3.3 Nanofluid models with different density of nanoparticles

As shown in Figure 36 to Figure 39, before the occurrence of fiction convergence in all models with different nanoparticles and roughness, models with multiple particle nanofluids always show lower friction force than the single particle nanofluids, indicating that the concentration of the nanofluids is important in the lubrication process, which supports the conclusions of Ma et al. [18]. Higher concentration results in lower friction force for models before friction force converges.

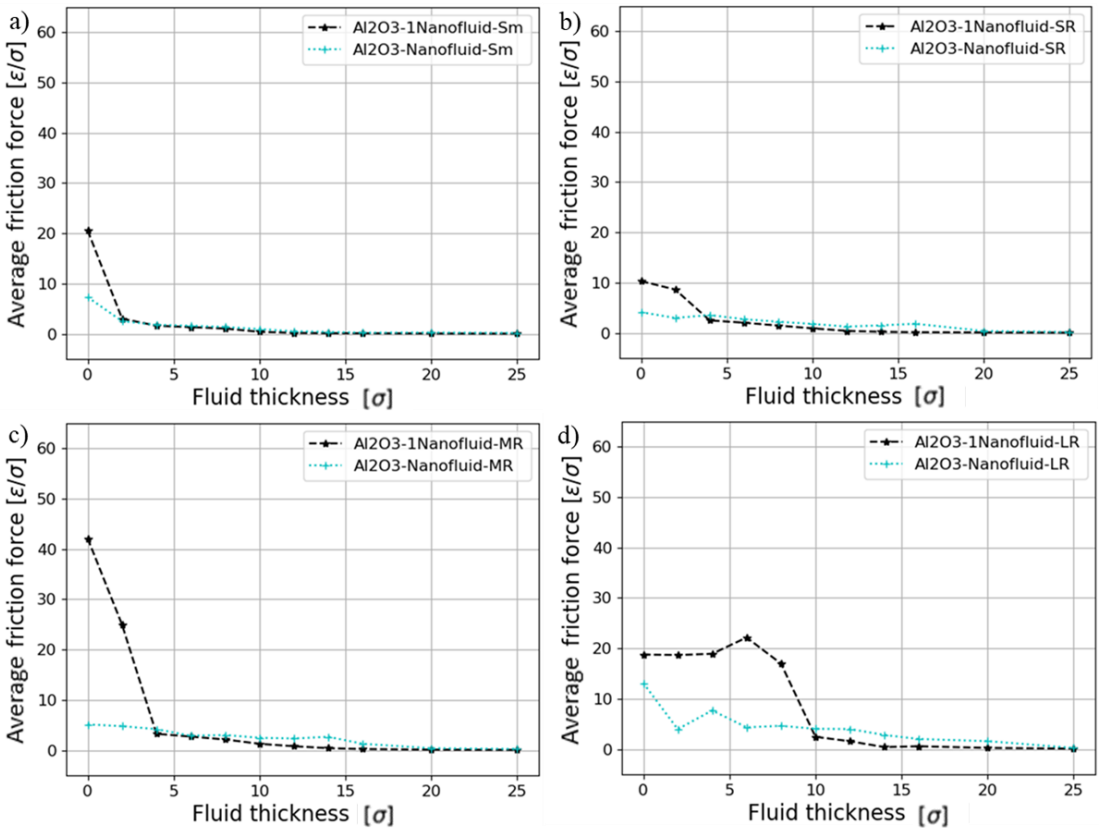

Figure 36 Friction force for a) smooth, b) small, c) medium and d) large rough surface models as a function of Al_2O_3 nanofluid thickness

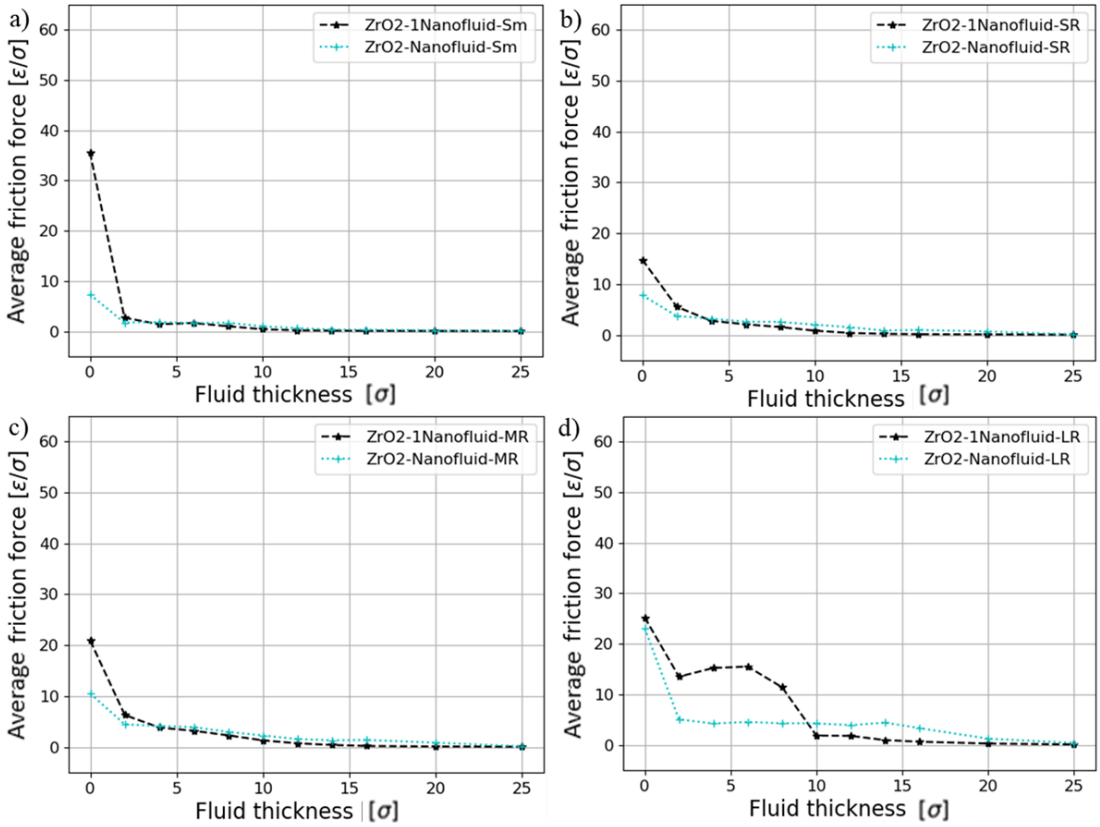

Figure 37 Friction force for a) smooth, b) small, c) medium and d) large rough surface models as a function of ZrO_2 nanofluid thickness

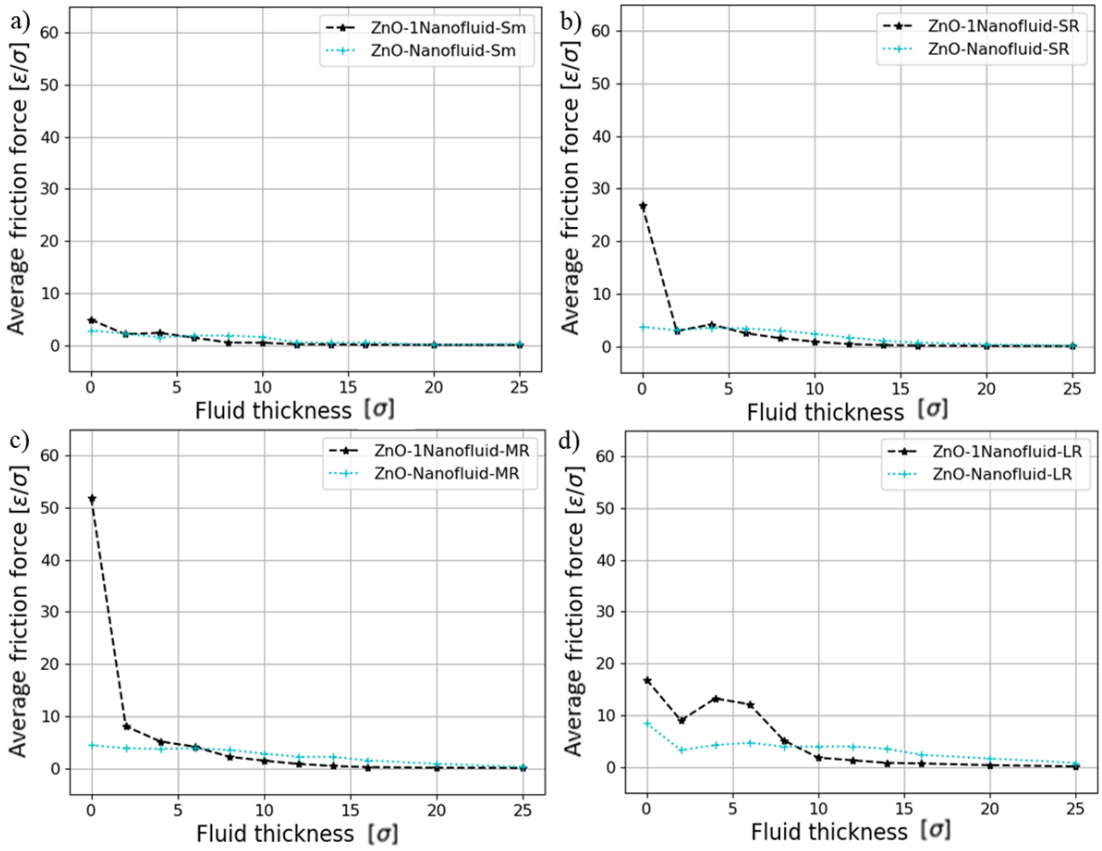

Figure 38 Friction force for a) smooth, b) small, c) medium and d) large rough surface models as a function of ZnO nanofluid thickness

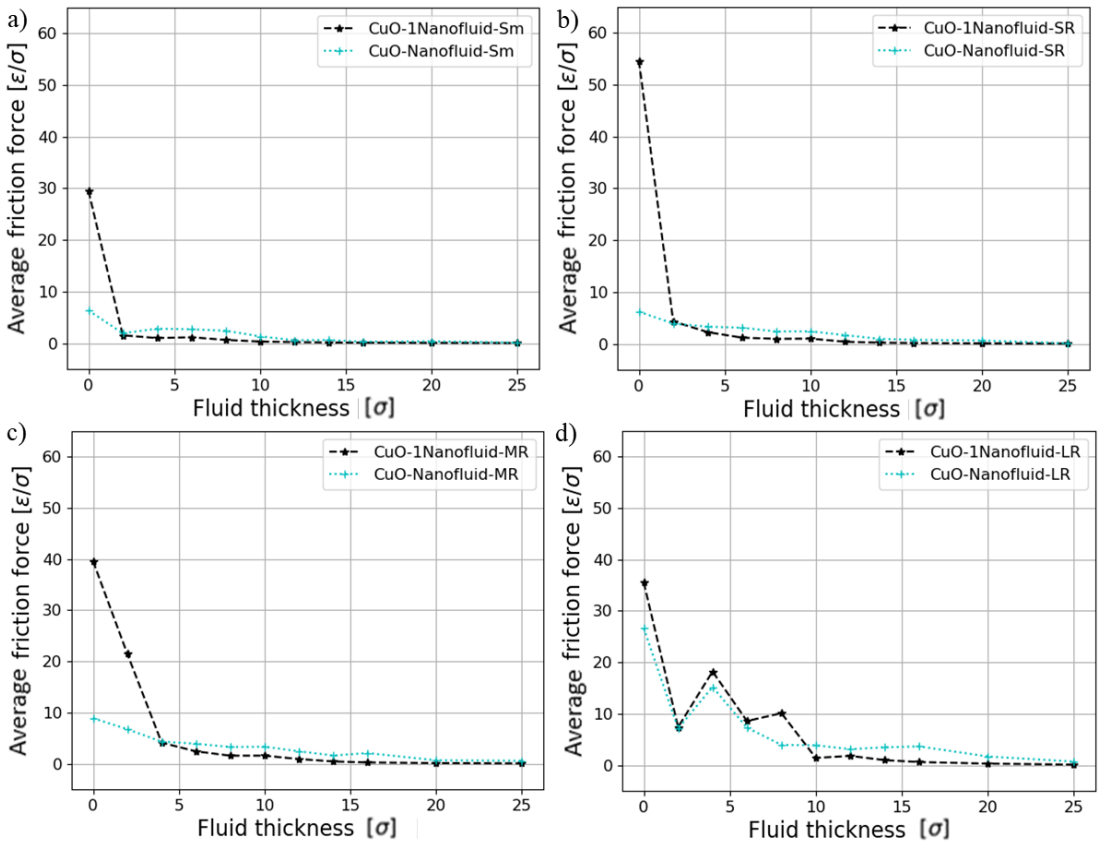

Figure 39 Friction force for a) smooth, b) small, c) medium and d) large rough surface models as a function of CuO nanofluid thickness

4.4 Discussion

The average friction force data first shown in Figs. 9, 12, 21, and 24, has been replotted as the percentage friction increase (or decrease) for two types of nanofluid (Al_2O_3 & ZnO) relative to the base fluid as a function of fluid thickness and roughness has been replotted in Fig. 40. For a given roughness and fluid thickness the percent friction increase is calculated as:

%Increase = (Friction with nanoparticles – Friction Base Fluid) / Friction Base Fluid x 100%

Negative values indicate a reduction in friction with respect to the base fluid, while positive values indicate an increase. From Fig. 40 a number conclusions can be drawn regarding the regimes where nanofluids may be most beneficial in reducing friction. First, nanoparticles (regardless of the initial surface roughness, nanoparticle type and number of nanoparticles) lower friction relative to the base fluid for dry conditions (0 fluid thickness). In all cases, dry friction results in almost complete destruction of the sliding interface rendering the identification of the cause of this reduction difficult. Second, in lubricant starved conditions (fluid thickness < roughness amplitude) multiple nanoparticles tend to lower friction relative to the base fluid. In such cases, the nanoparticles appear to act as a tribolayer which separates the opposing surfaces. Many researchers have pointed to tribofilm formation due to nanoparticles as a driving force for friction reduction [13, 17]. The nanoparticles also plastically deform the surface asperities which produces a smoother surface asperity. Third, individual nanoparticles (hard or soft) worsen friction at low and medium fluid thickness to a considerable degree. In the worst case, friction increases by a factor of ten (~1000%) in the presence of the multiple hard nanoparticles. As the fluid thickness increases, the negative effect of the nanoparticle on friction is reduced, especially for Sm, SR, and MR surfaces. For the LR surface, single nanoparticles have a beneficial effect on friction at fluid thicknesses > 10σ, offering approximately a 75% reduction in friction. Inspection of the atomic trajectories (Figs. 10 and 13) suggests that this enhancement

is due to plastic deformation and smoothing of the surface asperities. When multiple nanoparticles are present agglomerates form and these agglomerates block and lock between the rough surfaces (Figs. 22 and 25) and increase friction with respect to the base fluid. Previous MD simulations by Aminfar et al [40] suggest that increased interaction strength between nanoparticle and fluid helps to prevent nanoparticle agglomeration. In the present work, the interaction strength is weak and makes the nanoparticles likely to agglomerate. The effects of interaction strength were not investigated. Research has also shown that nanoparticles tend to increase fluid viscosity [33]. This may be the cause of the friction increase relative to the base fluid observed for smooth surfaces with multiple nanoparticles.

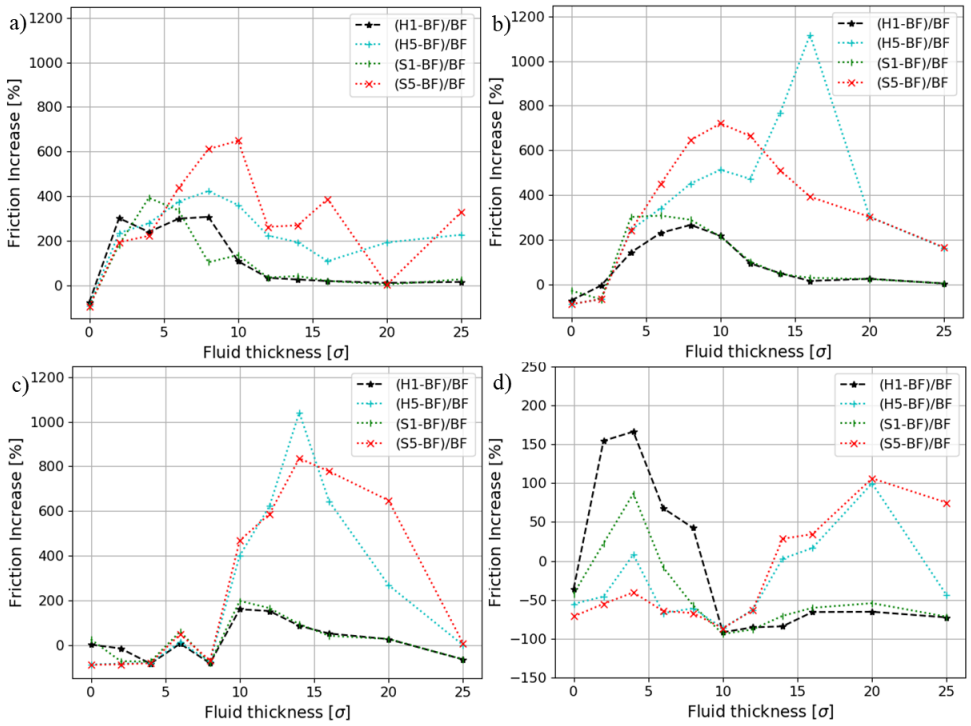

Figure 40 Relative friction as a function of fluid thickness for a) smooth surfaces, b) small roughness, c) medium roughness, and d) large roughness surfaces

CHAPTER FIVE

CONCLUSION AND FUTURE WORK

5.1 Conclusions

In this research, the MD simulation was conducted to investigate the tribological properties. Models lubricated with base fluid and Al_2O_3, ZrO_2, ZnO & CuO nanofluid between two solid surfaces with different surface roughness for molecular simulation were built. Several conclusions could be drawn from this research as follows:

1. When no fluid is present friction is highest for all 220 simulation models. For the smooth surface models lubricated by base fluid with no fluid, the friction force is equal to the theoretical interfacial shear strength of the material.
2. During dry contact the materials only interact at the asperity peaks so the friction of rougher surfaces models is lower than for smooth surface models due to the difference in true contact area. Transfer films were formed in all the rough surface models during dry contact. For models which contain base fluid, significant wear and smoothing of the asperities followed by fusion of the surfaces and generation of third body particles was found.
3. When a fluid is introduced into the interface the average friction force drops

significantly and the role of surface roughness is reversed. When the fluid thickness is equal to or larger than 2σ, the friction force reduces as the surface roughness decreases.

4. For models lubricated by nanofluid, the average friction force converges from different critical fluid thickness value as fluid thickness increases. The critical fluid thickness values of single and multiple particle nanofluid models are both 2σ for ZrO2 and 4σ for Al2O3, ZnO & CuO nanofluid.
5. During the impact and friction processes, nanoparticles in single particle nanofluid models rotate and translate under effects of the shear force from plates before plates contact with nanoparticles. While for multiple particle nanofluid models, nanoparticles would aggregate together serving as a supporting effect for surfaces and results in translational motion. The supporting effect reduces the contact of two plates, decrease friction force and strengthens the lubricating effect.
6. Before the occurrence of fiction convergence in all models with different nanoparticles and roughness, models with multiple particle nanofluids always show lower friction force than the single particle nanofluids, indicating that the concentration of the nanofluids is important in the lubrication process. Higher concentration results in lower friction force for models before friction force converges.

7. Except for medium rough surface models lubricated by single ZrO_2 nanofluid exhibit the lowest friction force. All the remaining models confined with single & multiple ZnO nanofluid always exhibit the lowest friction force for all models with different roughness before convergence occurs with increased fluid thickness. Except CuO particle, Al2O3, ZrO2 and ZnO particles have higher hardness than the solid steel surface. Within these three kinds of particles, ZnO particle has the most similar hardness value when compared with the hardness of the solid steel surfaces.
8. The deformation of nanoparticles depends on the hardness of the nanoparticle. Hard Al2O3 and ZrO2 particles on soft steel surfaces usually have small deformation and are more likely to roll and polish. Soft ZnO and CuO particles on soft steel surfaces have large deformation and are more likely to be squashed and form a film result in lower friction force.
9. Some atoms cut from the rough surface tips and deformed nanoparticles adsorbed to surfaces and have an effect of filling for rough surfaces, resulting in smoother surfaces producing lower friction force.
10. When the fluid thickness is large enough, the top surface will never contact the bottom surface. The friction mechanism will be different from those for models with less or totally no liquid.

5.2 Future work

Several suggestions for future work

1. To explore and determine the role of normal force in friction and wear by varying it.
2. There is a series of things that you can do to further analyzation of the simulation, including changes in roughness, changes in particle shape, particle rotation degree.
3. The interaction strength between the fluid and nanoparticles is weak in our simulations, which can be increased to see the results.

Reference

[1] Choi, S U.S., & Eastman, J A. (1995) Enhancing thermal conductivity of fluids with nanoparticles. United States. https://www.osti.gov/servlets/purl/196525

[2] Eastman, J A, Choi, U S, Li, S, Thompson, L J, & Lee, S. (1996) Enhanced thermal conductivity through the development of nanofluids. United States. https://www.osti.gov/servlets/purl/459378

[3] Jung, J., Oh, H., & Kwak, H. (2009). Forced convective heat transfer of nanofluids in microchannels. International Journal of Heat and Mass Transfer, 52(1), 466–472. https://doi.org/10.1016/j.ijheatmasstransfer.2008.03.033

[4] Uflyand, I., Zhinzhilo, V., & Burlakova, V. (2019). Metal-containing nanomaterials as lubricant additives: State-of-the-art and future development. Friction, 7(2),.93–116. https://doi.org/10.1007/s40544-019-0261-y

[5] Peng, D., Chen, C., Kang, Y., Chang, Y., & Chang, S. (2010). Size effects of SiO2 nanoparticles as oil additives on tribology of lubricant. Industrial Lubrication and Tribology, 62(2), 111–120. https://doi.org/10.1108/00368791011025656

[6] Chavan, D., & Pise, A. (2015). Experimental investigation of convective heat transfer agumentation using Al2O3/water nanofluid in circular pipe. Heat and Mass Transfer, 51(9), 1237–1246. https://doi.org/10.1007/s00231-014-1491-1

[7] F.H. Stott, & G.C. Wood. (1978). The influence of oxides on the friction and wear of alloys. Trib. Int., 11(4),.211–218. https://doi.org/10.1016/0301-679X(78)90178-0

[8] J. Jiang, F.H. Stott, M.M. Stack. (1998). The role of triboparticulates in dry sliding wear. Tribology International, 31(5),. 245-256. https://doi.org/10.1016/S0301-679X(98)00027-9

[9] H. Kato. (2003). Severe-mild wear transition by supply of oxide particles on sliding surface. Wear, 255,.426–429. https://doi.org/10.1016/S0043-1648(03)00077-2

[10] Gulzar, M., Masjuki, H., Kalam, M., Varman, M., Zulkifli, N., Mufti, R., & Zahid, R. (2016). Tribological performance of nanoparticles as lubricating oil additives. Journal of Nanoparticle Research: an Interdisciplinary Forum for Nanoscale Science and Technology, 18(8), 1–25. https://doi.org/10.1007/s11051-016-3537-4.

[11] Saidur, R., Leong, K.Y. and Mohamm, H.A. (2011). A review on applications and challenges of nanofluids. Renewable and Sustainable Energy Reviews, Vol.15(3),.1646-1668. https://doi.org/10.1016/j.rser.2010.11.035.

[12] Gara, L. and Zou, Q. (2012). Friction and Wear Characteristics of Water-Based ZnO and Al2O3Nanofluids. Tribology Transactions, 55(3),.345-350. https://doi.org/10.1080/10402004.2012.656879.

[13] Gara, L. and Zou, Q. (2013). Friction and Wear Characteristics of Oil-Based ZnO Nanofluids. Tribology Transactions, 56(2),.236-244. https://doi.org/10.1080/10402004.2012.740148

[14] Wu, Y. Y., Tsui, W. C., and Liu, T. C. (2007) Experimental Analysis of Tribological Properties of Lubricating Oils with Nanoparticle Additives, Wear, 262(7–8), 819–825. https://doi.org/10.1016/j.wear.2006.08.021

[15] Ma, Jianqi, and Mingwu Bai. (2009) Effect of ZrO2 Nanoparticles Additive on the Tribological Behavior of Multialkylated Cyclopentanes. Tribology Letters, 36(3), 191-198. https://doi.org/10.1007/s11249-009-9459-x

[16] Hernández Battez, A., González, R., Viesca, J., Fernández, J., Díaz Fernández, J., Machado, A., Chou, R. and Riba, J. (2008). CuO, ZrO2 and ZnO nanoparticles as antiwear additive in oil lubricants. Wear, 265(3-4),.422-428. https://doi.org/10.1016/j.wear.2007.11.013

[17] Kato, H. and Komai, K. (2007). Tribofilm formation and mild wear by tribo-sintering of nanometer-sized oxide particles on rubbing steel surfaces. Wear, 262(1-2),.36-41. https://doi.org/10.1016/j.wear.2006.03.046

[18] Guo, J., Barber, G., Schall, D., Zou, Q. and Jacob, S. (2017). Tribological properties of ZnO and WS_2 nanofluids using different surfactants. Wear, 382-383, pp.8-14. https://doi.org/10.1016/j.wear.2017.04.003.

[19] Ma, S., Zheng, S., Cao, D. and Guo, H. (2010). Anti-wear and friction performance of ZrO2 nanoparticles as lubricant additive. Particuology, 8(5),.468-472. https://doi.org/10.1016/j.partic.2009.06.007

[20] Chen, Q., Zheng, S., Yang, S., Li, W., Song, X. and Cao, B. (2012). Enhanced tribology properties of ZnO/Al2O3 composite nanoparticles as liquid lubricating additives. Journal of Sol-Gel Science and Technology, 61(3),.501-508. https://doi.org/10.1007/s10971-011-2651-0.

[21] Zulhanafi P, Syahrullail S, Faridzuan M M. (2017). Tribological performance of palm kernel oil added with nanoparticle copper oxide using fourball tribotester. Jurnal Teknologi, 79,.53-59. https://doi.org/10.11113/jt.v79.12265

[22] Luo, T., Wei, X. and Huang, X. et al. (2014). Tribological properties of Al2O3 nanoparticles as lubricating oil additives. Ceramics International, 40,.7143–7149. https://doi.org/10.1016/j.ceramint.2013.12.050.

[23] Casado, J., González, A., Huerga, Á., Rodríguez-Solla, H., Díaz-García, M., & Badía-Laíño, R. (2017). Unctuous ZrO2 nanoparticles with improved functional attributes as lubricant additives. Nanotechnology, 28(49),.1-11. https://doi.org/10.1088/1361-6528/aa93ca.

[24] Gu, Y., Zhao, X., Liu, Y., & Lv, Y. (2014). Preparation and Tribological Properties of Dual-Coated TiO_2 Nanoparticles as Water-Based Lubricant Additives. Journal of Nanomaterials, 2014(2014), 1–8. https://doi.org/10.1155/2014/785680

[25] Trajano, F., Moura, F. and Ribeiro, B. et al. (2014). Study of Oxide Nanoparticles as Additives for Vegetable Lubricants. Materials Research, 17(5), 1124-1128. https://doi.org/10.1590/1516-1439.228213

[26] V. Thottackkad, M., Rajendrakumar, P., & Prabhakaran Nair, K. (2014). Experimental studies on the tribological behaviour of engine oil (SAE15W40) with the addition of CuO nanoparticles. Industrial Lubrication and Tribology, 66(2), 289–297. https://doi.org/10.1108/ILT-01-2012-0006

[27] Bhaumik, S., Maggirwar, R., Datta, S., & Pathak, S. (2018). Analyses of anti-wear and extreme pressure properties of castor oil with zinc oxide nano friction modifiers. Applied Surface Science, 449, 277–286. https://doi.org/10.1016/j.apsusc.2017.12.131.

[28] Adil, L., Jacqueline, L. S., Guogang R. (2015). Simulation and experimental study of rheological properties of CeO2-water nanofluid. Int Nano Lett, Vol.5,.1-7. https://doi.org/10.1007/s40089-014-0129-0

[29] Adil, L., Jacqueline, L. S., Guogang R. (2014) The Approach of using Molecular Dynamics for Nanofluid Simulations. Intern. J. Eng.Res. Technol., Vol. 3(5),.1236-1247. https://doi.org/10.17577/IJERTV3IS051461

[30] Chengzhi, H., Minli, B., Jizu, L. and Xiaojie, L. (2015). Molecular dynamics simulation of mechanism of nanoparticle in improving load-carrying capacity of lubricant film. Computational Materials Science, Vol.109,.97-103. https://doi.org/10.1016/j.commatsci.2015.07.028

[31] Stephan, S., Lautenschlaeger, M., Alhafez, I., Horsch, M., Urbassek, H. and Hasse, H. (2018). Molecular Dynamics Simulation Study of Mechanical Effects of Lubrication on a Nanoscale Contact Process. Tribology Letters, Vol.66(4),.1-13. https://doi.org/10.1007/s11249-018-1076-0

[32] Chengzhi, H., Minli, B., Jizu, L., Zhihai, K. and Xiaojie, L. (2015). Molecular dynamics simulation on the tribology properties of two hard nanoparticles (diamond and silicon dioxide) confined by two iron blocks. Tribology International, Vol.90, 297-305. https://doi.org/10.1016/j.triboint.2015.04.043

[33] Chengzhi, H., Minli, B., Jizu, L., Peng W. and Xiaojie, L. (2014). Molecular dynamics simulation on the friction properties of nanofluids confined by idealized surfaces. Tribology International, Vol.78, 152-159. https://doi.org/10.1016/j.triboint.2014.05.018

[34] Rajabpour, A., Akizi, F., Heyhat, M., Gordiz, K. (2013) Molecular dynamics simulation of the specific heat capacity of water-Cu nanofluids. International Nano Letters, Vol.3(1), 1-6. https://doi.org/10.1186/2228-5326-3-58

[35] Hu, C., Lv, J., Bai, M. et al. Molecular dynamics simulation of effects of nanoparticles on frictional heating and tribological properties at various temperatures. Friction 8, 531–541 (2020). https://doi.org/10.1007/s40544-019-0271-9

[36] Lorenz, C., Lane, J., Chandross, M., Stevens, M., & Grest, G. (2009). Molecular Dynamics Simulations of Water Confined between Matched Pairs of Hydrophobic and Hydrophilic Self-Assembled Monolayers. Langmuir, 25(8), 4535–4542. https://doi.org/10.1021/la803940b

[37] Lane, J., Chandross, M., Lorenz, C., Stevens, M., & Grest, G. (2008). Water Penetration of Damaged Self-Assembled Monolayers. Langmuir, 24(11), 5734–5739. https://doi.org/10.1021/la703492j

[38] J. Lv, M. Bai, W. Cui, & X. Li. (2011) The molecular dynamic simulation on impact and friction characters of nanofluids with many nanoparticles system. Nanoscale Res Lett 6, 200. https://doi.org/10.1186/1556-276X-6-200

[39] Izadkhah, MS., Zeinali Heris, S. Influence of Al2O3 nanoparticles on the stability and viscosity of nanofluids. J Therm Anal Calorim 138, 623–631 (2019). https://doi.org/10.1007/s10973-019-08228-2

[40] H. Aminfar, N. Razmara, & M. Mohammadpourfard. (2015). Molecular Dynamics Study of Aggregation in Nanofluid Flow: Effects of Liquid–Nanoparticle Interaction Strength and Particles Volume Fraction. International Journal of Applied Mechanics. 07. 1550010. https://doi.org/10.1142/S1758825115400104

[41] Toroz, F. Song, G.A. Chass, & D.D. Tommaso. (2021). New insights into the role of solution additive anions in Mg2+ dehydration: implications for mineral carbonation. CrystEngComm. 23. https://doi.org/10.1039/D1CE00052G

[42] Yongcheng Zhou (2017). The effect of particle hardness on tribological properties of nanofluids

[43] Peter A. Thompson, & Mark O. Robbins. (1990). Origin of Stick-Slip Motion in Boundary Lubrication. Science (American Association for the Advancement of Science), 250(4982), 792–794. https://doi.org/10.1126/science.250.4982.792

[44] Thompson, P., Grest, G., & Robbins, M. (1992). Phase transitions and universal dynamics in confined films. Physical Review Letters, 68(23), 3448–3451. https://doi.org/10.1103/PhysRevLett.68.3448

[45] Thompson, P., & Robbins, M. (1990). Shear flow near solids: Epitaxial order and flow boundary conditions. Physical Review. A, Atomic, Molecular, and Optical Physics, 41(12), 6830–6837. https://doi.org/10.1103/PhysRevA.41.6830

[46] KOILLER, JI, H., & ROBBINS, M. O. (1992). Effect of disorder and lattice type on domain-wall motion in two dimensions. Physical Review. B, Condensed Matter, 46(9), 5258–5265. https://doi.org/10.1103/PhysRevB.46.5258

[47] NOLLE, KOILLER, B., MARTYS, N., & ROBINS, M. O. (1993). Morphology and dynamics of interfaces in random two-dimensional media. Physical Review Letters, 71(13), 2074–2077. https://doi.org/10.1103/PhysRevLett.71.2074

[48] C.S. Nolle, Belita Koiller, Nicos Martys, Mark O. Robbins. (1994). Effect of quenched disorder on moving interfaces in two dimensions, Physica A: Statistical Mechanics and its Applications, Volume 205, Issues 1–3, 342-354, https://doi.org/10.1016/0378-4371(94)90512-6.

[49] Luan, B., Hyun, S., Robbins, M., & Bernstein, N. (2004). Multiscale Modeling of Two Dimensional Rough Surface Contacts. MRS Proceedings, 841, R7.4. https://doi:10.1557/PROC-841-R7.4.

[50] M. P. Allen & D. J. Tildesley. Computer Simulation of Liquids. New York, Oxford University Press, 1987.https://doi.org/10.1093/oso/9780198803195.001.0001

[51] J.M. Ian. Dictionary of Ceramic Science and Engineering. 3rd ed. 2013, 17-527. Springer Netherlands. https://doi.org/10.1007/978-94-007-0916-4

[52] Stephan, S., Staubach, J., & Hasse, H. (2020). Review and comparison of equations of state for the Lennard-Jones fluid. Fluid Phase Equilibria, 523, 112772–112795. https://doi.org/10.1016/j.fluid.2020.112772

[53] https://lammps.sandia.gov/doc/Howto_thermostat.html

[54] M.O. Robbins, and Muser, M. H., in: B. B. (Ed.), Modern Tribology Handbook, Boca Raton, 2001, 717-771.

[55] https://lammps.sandia.gov/

[56] https://www.ks.uiuc.edu/Research/vmd/

[57] P.C. Bernal, J.D. Schall, J.A. Harrison, Y.-R. Jeng, & R.W. Carpick. (2018). Influence of chemical bonding on the variability of diamond-like carbon nanoscale adhesion. Carbon (New York), 128, 267–276. https://doi.org/10.1016/j.carbon.2017.11.040